

Supplementary information

The overestimated capability of fluid shear to induce secondary nucleation: an urgent call for diligently executed control experiments

Lorijn De Vrieze and Simon Kuhn*

KU Leuven, Department of Chemical Engineering, 3001 Leuven, Belgium

E-mail: simon.kuhn@kuleuven.be

Contents

S1 - Critical overview of control experiments in literature	2
S2 - Description of the experimental setup	12
S3 - Seed crystal preparation - washing procedure	18
S4 - Solution preparation and experiment initialization	25
S5 - Characteristics of experiment I	26
S6 - Characteristics of experiment II	30
S7 - Characteristics of experiment III	34
S8 - Characteristics of experiment IV	40

S1 - Critical overview of control experiments in literature

It is claimed in the main document that the control experiments for (i) *initial breeding* and (ii) *primary nucleation* are often overlooked in literature. To support this, a list of identified works stating to have experimentally observed fluid shear-induced secondary nucleation is provided here. Moreover, the control measures that were installed are verified for each work after a short description of the experimental setup. The color **green** shows a correctly executed control experiment, while **red** indicates a detected inconsistency.

Needless to say, missing details in described experimental procedures from literature make it challenging to judge all works correctly. The following list thus incorporates educated opinions from the authors of this article. Although it clearly highlights the general lack of diligently executed control experiments, potential misjudgments are unintentional. **The principal goal of this article is to raise awareness of a pressing issue in the field and to stimulate a constructive discussion on the topic.**

In contrast to the listed research papers, there are *only a few experimental works observing that fluid shear could not induce secondary nucleation*. These are the works from Lal and Strickland-Constable,¹ Tait and Litster,² and Steendam.³ Although they reported the absence of fluid shear-induced secondary nucleation and even linked it with inconsistencies in some control experiments, they failed to provide a full picture of the (absence of) control experiments in literature as was demonstrated in this article. Nevertheless, their important findings will be included in this list.

Powers (1956)⁴ - <https://doi.org/10.1038/178139a0>

This experiment is extensively addressed in the main document.

short description A single large sucrose crystal was attached to a rod, which is placed in solution and rotated around its axis. The rotation of this crystal caused “nucleation to be produced virtually in a [super]saturated solution at high enough spinning rates”.

initial breeding No pretreatment or washing of the large sucrose seed crystal has been reported, and thus initial breeding could occur. A similar observation has previously been reported by Lal and Strickland-Constable¹.

primary nucleation When a “Perspex model” was used, i.e. a piece of PMMA with same shape as the used sucrose seed crystal, nucleation was detected to be slower compared to when the actual seed crystal was used.

Denk and Botsaris (1972)⁵ - [https://doi.org/10.1016/0022-0248\(72\)90287-4](https://doi.org/10.1016/0022-0248(72)90287-4)

short description A single NaClO₃ seed crystal was added to either a stagnant aqueous supersaturated solution, or fixed into a tube and subjected to flow. Afterwards, the polarity of the formed crystals was analyzed. No induction times or number of produced crystals were recorded. The observed deviation from 50%/50% *l*-NaClO₃/*d*-NaClO₃ (primary nucleation) was explained as fluid shear-induced secondary nucleation.

initial breeding For all experiments “pretreated seed crystals” were used, indicating a washing step of some sort. However, more experimental details on the washing procedure are missing. With the work of Steendam³ and the only recent awareness of initial breeding at that time⁶ in mind, it seems highly likely that initial breeding was not fully eliminated.

primary nucleation The supersaturation was altered over a wide range, up to primary nucleation conditions (50%/50% *l*-NaClO₃/*d*-NaClO₃). Combined with the use of a glass object of the same size as the used crystals, primary nucleation was accurately avoided.

Sung and Youngquist (1973)⁷ - <https://doi.org/10.1002/aic.690190511>

short description A magnesium sulfate crystal was mounted on a stick and placed in a supersaturated solution 1.8 mm away from a large impeller. After rotating for 30 s (high shear pulse), the solution was cooled and the number of produced crystals counted.

initial breeding The seed crystals were pretreated for 30 min in an undersaturated solution. This paper was a reply to the work from Lal and Strickland-Constable,¹ who brought seed “pretreatment” to mainstream attention. It is thus acceptable to conclude that the authors will have ensured that initial breeding was out of the picture.

primary nucleation Only one single experiment was conducted in absence of a seed crystal, insufficient to decide whether there is interference from primary nucleation or not. Also, no object was placed near the stirrer in the primary nucleation control experiment to compensate for the higher fluid shear values by seed introduction.

Estrin and Youngquist (1975)⁸ - <https://doi.org/10.1002/aic.690210225>

short description A jet system was deployed to subject a polycrystalline ice seed crystal to high fluid shear values. After jetting, the solution was transferred into a vial at lower temperature to speed up the growth process of the formed crystals.

initial breeding The ice seed was pretreated to avoid initial breeding by “immersion in [undersaturated] solution at room temperature”. Although further details are missing, it remains acceptable that initial breeding was eliminated as some of the authors of this work already have publications with correctly executed initial breeding control experiments.

primary nucleation Only three primary nucleation control experiments were conducted using a “dummy crystal from hard rubber”. The number of control experiments is thus too low for primary nucleation to be absent here.

Jagannathan and Estrin (1980)⁹ - No DOI available

Though often cited by other works in this list, this paper could not be obtained.

Only educated guesses can thus be made on the accuracy of the adopted control experiments.

short description A “momentary jet of supersaturated [aqueous] solution” was released upon a stationary seed crystal of magnesium sulfate or potassium aluminum sulfate. Afterwards, the solution was cooled to observe the nucleated crystals.

initial breeding One of the authors of this work is Estrin, which also (co-)authored other instances^{7,8} in this list. Since initial breeding control experiments were conducted correctly before, one can presume that a similar procedure was followed here as well.

primary nucleation Again, in the light of the previous two works (co-)authored by Estrin, only a limited number of control experiments were conducted, insufficient to rule out any interference. Although the jet might have been used when screening for the presence of primary nucleation, it seems likely that no object was used to mimic locally enhance fluid shear values caused by the presence of a stagnant object.

Wang and Yang (1981)¹⁰ - <https://doi.org/10.1080/00986448108910840>

short description A Couette cell was constructed to subject a solution of ϵ -caprolactam in toluene to constant fluid shear values. After introducing a seed-on-a-stick in the annular gap, the Couette cell was rotated for 30 sec (shear pulse). Afterwards, the Couette cell was cooled in order to grow and detect the formed crystals.

initial breeding The used seed crystals are washed with solvent before each experiment. Although further details are missing, it appears likely that initial breeding has been eliminated in these experiments.

primary nucleation To ensure the absence of primary nucleation, only one control experiment has been conducted. Although a rubber object in the shape of the seed crystal has been used, the number of control experiments remains too low to avoid interference.

Wang and Estrin (1981)¹¹ - <https://doi.org/10.1002/aic.690270222>

short description A Couette cell has been fabricated to study the system of citric acid in water. After introduction of the seed-on-a-stick, the Couette cell was rotated for 30 sec (high shear pulse) and further cooled down for crystal growth.

initial breeding All seed crystals were pretreated by immersing them in distilled water (solvent) for 2 min before carefully sliding them into their place in the Couette cell.

primary nucleation To ensure the absence of primary nucleation, only one single primary nucleation control experiment has been conducted. Although a “dummy” was used, one single control experiment does not fully prove the absence of primary nucleation.

Youngquist (1987)¹² - <https://doi.org/10.1016/B978-0-08-035751-5.50013-1>

short description A “momentary jet of aqueous solution” was used to induce fluid shear on the a crystal face of a stationary magnesium sulfate or potassium alum seed crystal. After jetting, the solution around the seed crystal is directly transferred into another vial at lower temperature to grow the formed secondary crystals.

initial breeding Although it is mentioned that the jet was aimed at a “pretreated crystal face”, no further details on the washing procedure are provided. However, the work from Lal and Strickland-Constable¹ on magnesium sulfate shows how precisely the washing procedure of magnesium sulfate needs to be executed to avoid initial breeding.

primary nucleation To screen for primary nucleation, the seed crystal was replaced by a “dummy made from Plexiglass”. No crystals were observed in any of the experiments when the “dummy” was present, indicating an absence of primary nucleation.

Wang and Estrin (1996)¹³ - <https://doi.org/10.1080/00986449608936568>

short description A sucrose seed crystal was mounted on a rod and introduced into an aqueous supersaturated solution. The experimental setup consisted of two well-stirred sections: the upper part containing the seed crystal, and a lower part at a lower temperature. After 1 h in the upper section, the solution is transferred into the lower part. Crystals resulting from fluid shear-induced secondary nucleation are thus allowed to grow.

initial breeding The used seed crystals were submersed in an undersaturated solution for 20 min before introduction in the supersaturated solution, eliminating initial breeding.

primary nucleation It was tested that primary nucleation did not occur in the selected time intervals or by transferring the solution from one part to the other. However, no similar-sized object as a seed crystal has been deployed in these control experiments.

Qian and Botsaris (1998)¹⁴ - [https://doi.org/10.1016/S0009-2509\(98\)00040-2](https://doi.org/10.1016/S0009-2509(98)00040-2)

short description Using an isothermal seed-on-a-stick approach, secondary nucleation of NaClO_3 in water was studied. After introduction of the seed crystal in the supersaturated solution, the solution was kept stirred till crystals were observed. No induction times were reported. The polarity of these formed crystals was analyzed in function of the applied supersaturation. This way, a region next to the MSZW was found where the polarity of the formed crystals deviated from the seed crystal polarity, attributed to secondary nucleation by solely fluid shear.

initial breeding Although an extensive washing procedure is in place (both solvent washed and solution washed crystals were tested and give the same results), the seed crystal was held during the experiments using a rod with a split end. As demonstrated by Steendam³ while working with the same compound, this would probably already suffice to cause initial breeding since the crystal can slightly move in between the split.

primary nucleation Despite the conducted control experiments for primary nucleation, the number of these is insufficient (max 4 experiments were done) to avoid interference from primary nucleation. Moreover, the interesting observations were mainly made in a region next to the MSZW (primary nucleation), rendering these control experiments even more important. No inert object was used in the control experiments as well.

Buhse and Kondepudi (2000)¹⁵ - <https://doi.org/10.1103/PhysRevLett.84.4405>

short description A stationary NaBrO_3 crystal was held in place while a supersaturated solution of NaClO_3 in water was dripped over the seed crystal. The solution was collected and stored to let the water evaporate. Afterwards, the polarity of the formed

NaClO₃ crystals was analyzed. The deviation from 50%/50% *l*-NaClO₃/*d*-NaClO₃ here served as proof that fluid shear alone could induce secondary nucleation.

initial breeding The seed crystal was in this work held by a pair of tweezers. However, as demonstrated by the paper from Steendam³ on initial breeding of NaClO₃, even the slightest mechanical impact already suffices to cause initial breeding. Likewise, this explains the observed deviation from 50%/50% *l*-NaClO₃/*d*-NaClO₃, raising questions whether in this case fluid shear alone indeed could cause secondary nucleation.

primary nucleation Multiple control experiments were conducted using NaCl, an achiral seed crystal. This way, it was checked that the deviation from the 50%/50% *l*-NaClO₃/*d*-NaClO₃ resulted from the presence of the NaBrO₃ seed crystal. Similar fluid shear values were thus present for the control experiments (same sized crystal).

Tai and Chang (2009)¹⁶ - [https://doi.org/10.1016/0022-0248\(92\)90636-W](https://doi.org/10.1016/0022-0248(92)90636-W)

short description The used setup consisted of a stirrer tank with a syringe submerged in it. By altering the time between stopping the rotation and jetting (injection of solution directly on seed crystal with the syringe), the interfacial concentration was altered. Since no nucleation was detected after a long stopping time, it was claimed that the interfacial concentration was too low for the jet (fluid shear) to cause secondary nucleation.

initial breeding All used seed crystals are pretreated by dissolving them in the solution at 1°C above saturation temperature for 30 min (thus slowly dissolving in solvent).

primary nucleation The authors themselves mention that “to find proper supersaturation and agitation speed, we encountered a dilemma”. They were well aware that primary nucleation could interfere their experiments, especially with the desired high agitation rates and supersaturation. Numerous “induction time” experiments were thus executed to find the conditions as near as possible to primary nucleation, while still ensuring its absence. However, they did not deploy the jet (syringe) in these experiments, which

would very likely have led to higher fluid shear values. As a results, they probably also observed primary nucleation in their secondary nucleation experiments.

Yousuf and Frawley (2018)¹⁷ - <https://doi.org/10.1021/acs.cgd.8b01074>

This experiment is extensively addressed in the main document.

short description Applying a seed-on-a-stick approach, a large single paracetamol (PCM) seed crystal was introduced in an isopropyl alcohol (IPA) solution. A polythermal approach was used to show that the presence of the seed leads to faster onset of nucleation.

initial breeding The PCM seed crystal was washed using the anti-solvent cyclohexane. In contrast to washing with solvent, this method does not remove all crystalline fines.

primary nucleation Numerous control experiment for primary nucleation were carried out and the polythermal method allows to clearly distinguish a difference between runs with and without seed crystal. However, the primary nucleation control experiments were not carried out using an inert object in the same shape as the seed crystal, thus not compensating for locally increased fluid shear values.

Cashmore and Sefcik (2024)¹⁸ - <https://doi.org/10.1021/acs.cgd.4c00130>

short description To ensure constant fluid shear values, a custom-made Couette cell was used to study nucleation of glycine in water. A seed-on-a-stick approach was adopted in which an α -glycine crystal is introduced in the annular gap before rotation commenced. An isothermal approach is applied and snapshots of the solution are regularly taken to determine the onset of nucleation and to track its progress.

initial breeding The used seed crystals were washed by flowing 15 mL of solvent over the seed crystal, thus removing any crystalline debris present.

primary nucleation Apart from the secondary nucleation experiments, multiple primary nucleation experiments were also conducted. This would allow to clearly see a

difference in induction times between both (despite induction times for the secondary nucleation case not being reported). However, the annular gap in this setup is only 4 mm, while the introduced seed crystal is 2 mm in size. Such large object is thus very likely to alter the laminar flow field in the annular gap, significantly increasing local fluid shear values (as was also shown in the paper itself using CFD simulations). However, the primary nucleation control experiments were conducted without an inert object of the same shape as an α -glycine seed crystal present.

Important note on a cooling step after applying high fluid shear

A large portion of the fluid shear-induced secondary nucleation papers has developed the peculiar habit of lowering the solution temperature after having applied high fluid shear values on the seed crystal. This predominantly involves the short-pulsed fluid jet papers (Sung and Youngquist;⁷ Estrin and Youngquist;⁸ Jagannathan and Estrin;⁹ Wang and Yang;¹⁰ Wang and Estrin;¹¹ Youngquist¹²), which typically include an extra cooling step “to speed up the growth process of the formed crystals”.

However, as stated in several of these publications, **this extra temperature lowering step turns out to be a prerequisite for making fluid shear-induced secondary nucleation possible**. No extra temperature lowering step after the high shear pulse resulted in no secondary crystals formed. This striking observation is in sharp contrast with the remaining papers in the field, which state that fluid shear-induced secondary nucleation takes place in isothermal nucleation experiments as well.

This points out that there is a large discrepancy present in current literature on fluid shear-induced secondary nucleation, further stressing the importance of well-designed control experiments. Before drawing fundamental conclusions on secondary nucleation by fluid shear (e.g. the need for an extra cooling step), its isolation from all other interfering nucleation phenomena has to be guaranteed.

Important note on fluid mechanical impact and dendritic growth

In order to find fluid shear-induced secondary nucleation, the common trend is to deploy as high as possible fluid shear values and supersaturation^{19,20}. However, one should also realize that there is a maximum limit to possible fluid shear values and supersaturation.

Once the fluid shear forces acting on the seed crystal surface become too large, they can start breaking off crystalline pieces from the seed crystal. This *fluid mechanical impact* might be experimentally detected as fluid shear-induced secondary nucleation, while it is actually **nothing other than crystal breakage or attrition**.

On top of that, performing secondary nucleation experiments at too high supersaturation can cause small needle-like crystalline structures to start growing on the seed crystal surface in a process called *dendritic growth*. Once this occurs, even moderate fluid shear values suffice to break off these brittle protruded crystalline needles. New crystals formed under such conditions **should again be attributed to attrition** rather than fluid shear-induced secondary nucleation.

The work from Lal and Strickland-Constable¹ on $\text{MgSO}_4 \cdot 7\text{H}_2\text{O}$ showcases how little supersaturation is needed for dendritic growth to manifest itself ($\Delta T = 4^\circ\text{C}$). Consequently, this raises questions on the tests from Sung and Youngquist;⁷ Jagannathan and Estrin;⁹ and Youngquist¹² as they used the same chemical compound without mentioning or checking for the presence of dendritic growth.

S2 - Description of the experimental setup

Despite procedural differences, the utilized experimental setup was the same in all four conducted experiments (see S5 - S8). This section will discuss how this common part was constructed and operated. Overall, the setup consists of five units, as discussed further below, each with a specific purpose as demonstrated in Figure S1.

1. Crystallization unit

All crystallization experiments were conducted in custom-made double-jacketed cylindrical glass cups ($\varnothing 32$ mm; 40 mm height) filled with 20 mL solution (25 mm liquid height). The need for numerous nucleation experiments resulted in deploying ten identical crystallizers to speed up data generation. This crystallization unit stands central in the setup; the other units have as sole purpose to ensure desired experimental conditions in the crystallizers, either (2) temperature, (3) stirrer positioning, (4) RPM control, or (5) nucleation detection.

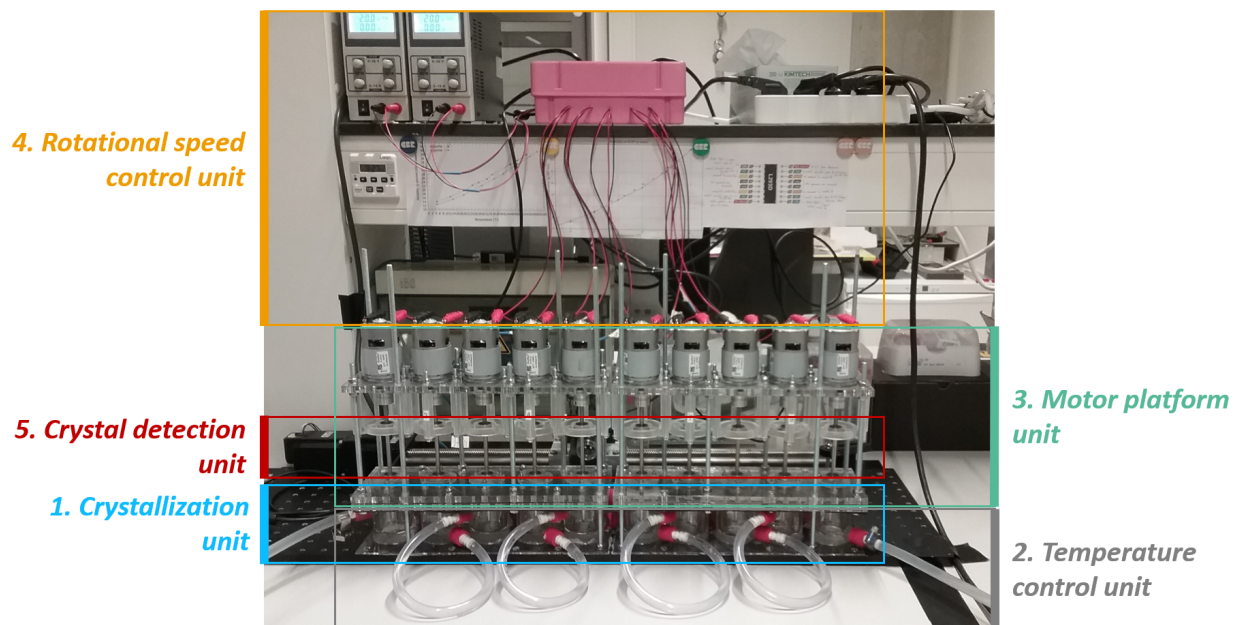


Figure S1: Overview picture of the experimental setup, subdivided in multiple units corresponding to their specific function.

2. Temperature control unit

Since the glass cups were double-jacketed, water from a recirculating bath (Huber Unichiller) was pumped in the annular gap for accurate temperature control. To avoid the use of multiple recirculating baths, the ten crystallizers were connected in series (silicone tubing and GL14 removable hose connections). For polythermal nucleation experiments, the linear cooling profile was established by the software installed on the recirculating water bath (Huber Pilot One with E-grade). By applying a thermocouple (RS Pro 363-0294, K-type) connected to a thermologger (Omega HH374), the temperatures were verified, displayed, and recorded during nucleation experiments.

3. Motor platform unit

All conducted experiments rely to some degree on a rotational movement (either mixing near or spinning of the seed crystal). Therefore, a framework had to be constructed that would allow different overhead stirrer types to be swapped in between experiments. As all spinning elements required in the four experiments could be attached to a 15 cm long stainless steel rod ($\varnothing 5$ mm), this was selected as the exchangeable element (see S3).

This rod was connected to the 5 mm motor shaft of a brushed DC motor (RS Components 877-6269, Mellor Electric, 24 V, 3500 RPM, 0.046 Nm, 13.6 W) using a 5 mm flexible shaft coupling (RS Components 814-590, Ruland Beam Coupling). To avoid eccentricity and excessive vibrations, a rigid structure was required to keep all spinning elements aligned. A robust platform was thus constructed using 8 mm thick acrylic plates (with lasercut holes, Trotec Speedy 100R), M6 stainless steel lead screws, and 3D printed structural elements (FormLabs Form 3, Clear V4 resin RS-F2-GPCL-04; modeled and blueprinted using Solid Edge, Siemens). The DC motors were screwed upon the top plate, while 3D printed holders incorporating 5 mm ball bearings (RS Pro 261-2632, deep groove closed end type) were positioned in between the top and bottom plate (see Figure S2). The use of a rubber O-ring when mounting the 3D printed holders on the acrylic plate allowed for precise alignment of



Figure S2: **left:** Picture of the motor platform unit. This rigid construction eliminates eccentricity and ensures reproducible positioning of the overhead stirrers. **right:** Close-up of the bottom 3D printed holder, highlighting holders where the “seed-on-a-stick” can be inserted and secured.

these ball bearings. The bottom 3D printed holder also served a dual purpose as holder for a “seed-on-a-stick”. The presence of a glued perpendicular female screw in the print allowed to clamp a 3 mm stainless steel stick with an attached seed crystal in the holder using a screw (see Figure S2).

The platforms themselves (two in total to ease handling, 30 cm length) fit over long stainless steel lead screws inserted in an aluminum breadboard plate (Thorlabs MB3090/M) to guarantee a consistent positioning of the overhead stirrers between experiments. One platform as a whole (acrylic plates with motors and overhead stirrers attached) can thus be lifted and placed on top of five crystallizers. The movement of these crystallizers is restricted since they are taped to the aluminum breadbord while also held in place by a 2 mm thick acrylic plate with cut-outs for the crystallizers. When performing experiments, the platform rests on top of the crystallizers: a rubber sheet was attached under the bottom acrylic plate to flatten out any unevenness and to limit solvent evaporation (see Figure S3).

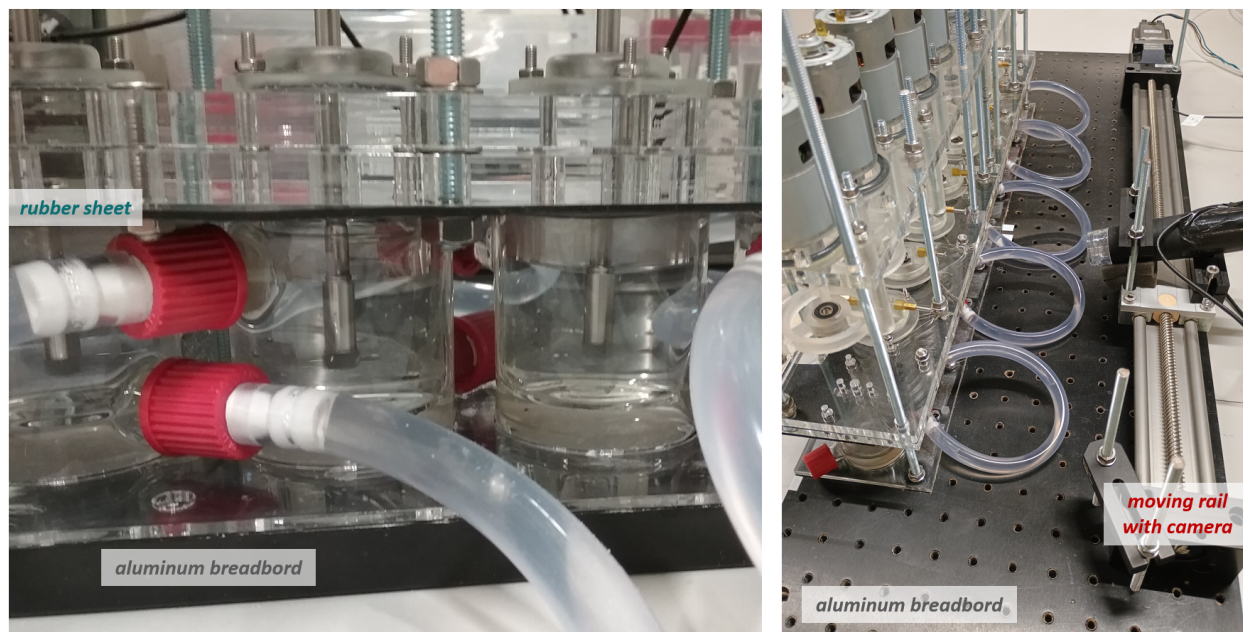


Figure S3: **left:** Close-up picture of a few crystallizers. The rubber sheet attached to the bottom of the motor platform unit serves as lid. **right:** The working principle of the crystal detection unit. By periodically moving the camera mounted on the rail, a snapshot can be taken of each crystallizer, allowing parallel operation.

4. Rotational speed control unit

The rotational speed of a DC motor is by definition linearly correlated with the applied voltage. Generating a calibration curve (see Figure S4) thus allowed revolutions per minute (RPM) of the stirrers to be precisely controlled. When calibrating, these RPM values were measured using an optical tachometer (RS Pro AT-6, 193-8687) on an unloaded DC motor.

However, each motor is unique, resulting in small deviations from the measured calibration curve. To ensure identical RPM values throughout all experiments, a high-speed camera (Fastcam Mini UX100, Photron) with microlens (Navitar 12X 1-50486) was used to verify RPM values when the motors were spinning in representative experimental conditions. To adapt for small deviations, the motors were wired up to a microprocessor (Arduino ATmega2560-R3) via DC motor drivers (L923D push-pull dual-channel H-bridge, STMicroelectronics). This allowed to precisely adjust the rotational speed using the signal sent by the microprocessor (see Figure S4 for a minimal version of the circuit diagram).

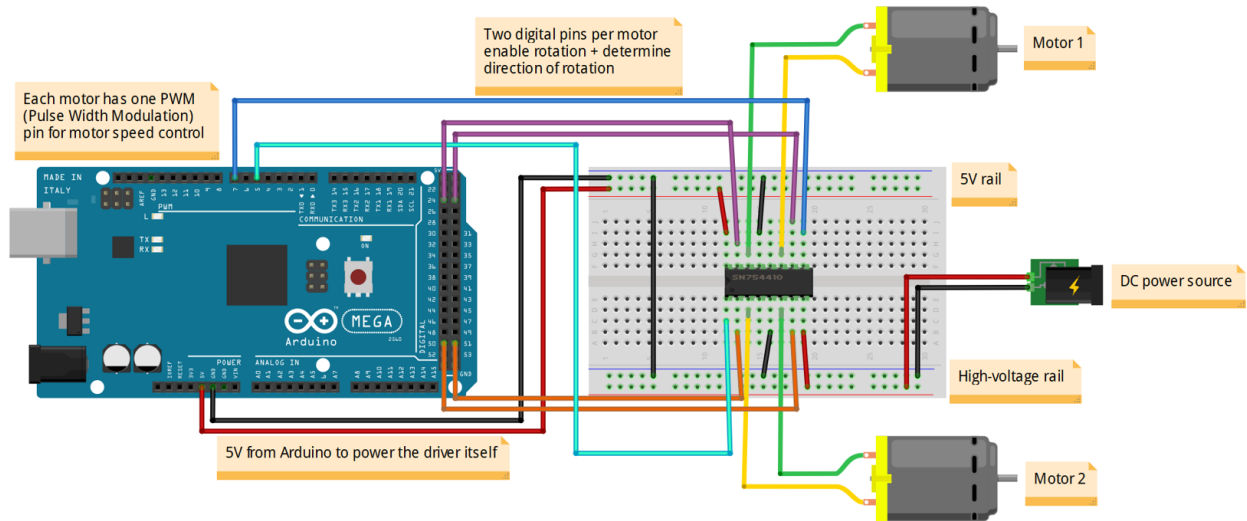
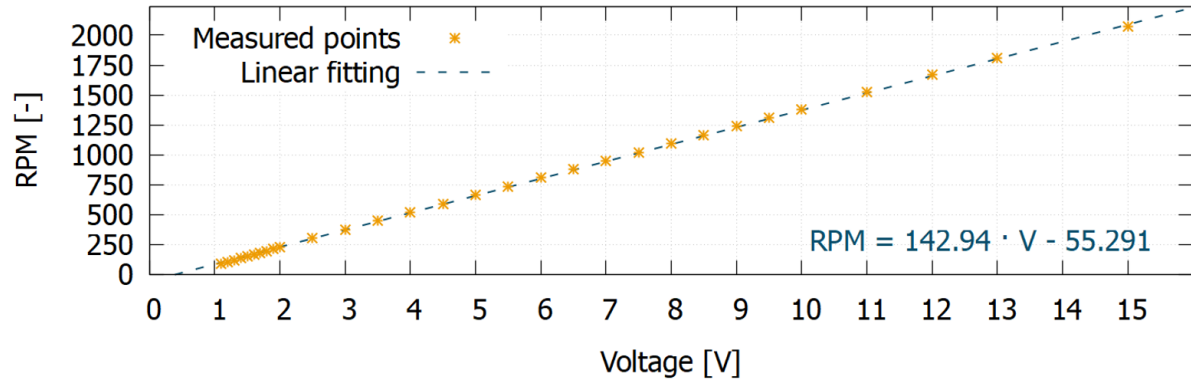


Figure S4: top: Measured calibration curve to link the set voltage with the RPM of the DC motors. bottom: Schematic representation of the rotational speed control unit involving a microprocessor (Arduino Mega) and DC motor driver. Each driver can independently transmit the speed regulating signal from the microprocessor to two motors. The real-life electrical circuit in place powers all ten DC motors at once using a single microprocessor.

Besides enabling little RPM tweaks, the incorporation of a microprocessor also allowed for a more complex spinning pattern (see S8). This was programmed in the open source Arduino IDE software before being compiling into runnable C++ code. Since the microprocessor could not provide sufficient power to run all ten DC motors at full capacity, two adjustable DC power sources (Velleman, 0-30 V, 0-10 A, 300 W) were made use of (wired to the motors through the motor drivers to protect the microprocessor from back EMF pulses).

5. Crystal detection unit

Optical access of the crystallizer contents was ensured by constructing the crystallizers fully out of glass and using water as coolant. The use of ten of them in parallel, however, makes simultaneous observation challenging. Here, a rail (Drylin SAW linear axis from Igus with a stroke length of 50.0 cm, driven by a NEMA23 stepper motor and controlled by a Dryve D1 Motor Controller) was deployed. By carrying a little camera (RS Pro 913-2480, USB digital microscope) and periodically moving the rail, a snapshot of each reactor could be taken every predetermined time interval (see Figure S3). Since the rail movement was synchronized with an automatic screenshot taking program (Auto Screen Capture by [gavinkendall](#)), the screenshots were afterwards sorted by crystallizer using a home-made Python script. By scrolling through the sorted pictures, the formation of the first crystal could be visually detected with an accuracy of 4 min (isothermal) or 0.4°C (polythermal). A typical nucleation experiment is displayed in Figure S5. Since the time of capturing was selected as file name, induction times could also be extracted for further analysis.

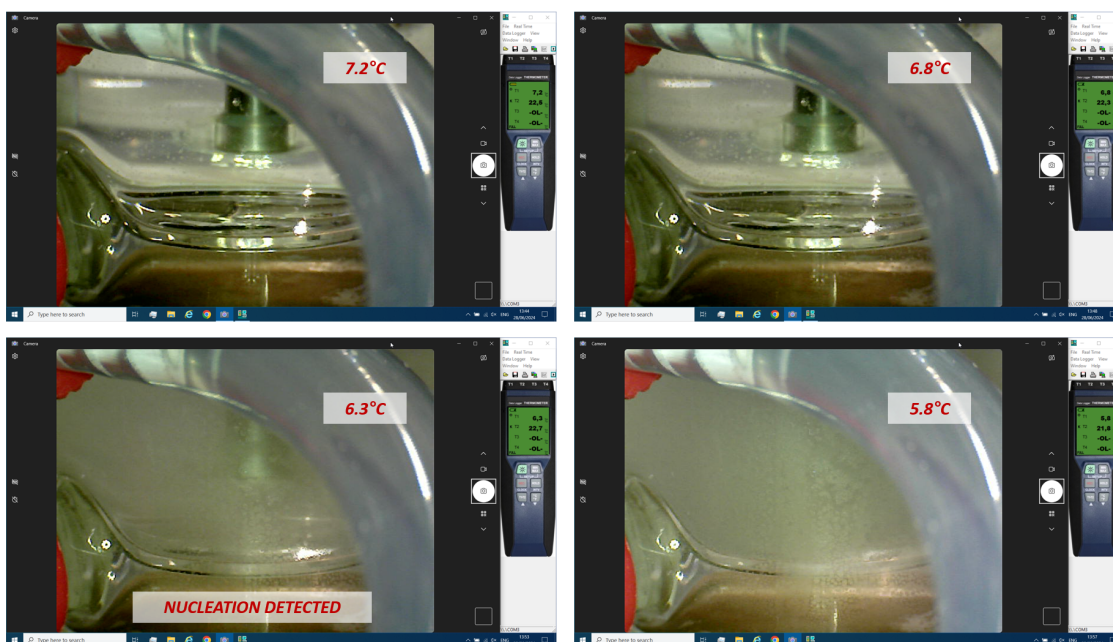


Figure S5: Pictures from a polythermal nucleation experiment, showcasing the detection of the onset of nucleation. By displaying the temperature, the MSZW could be determined.

S3 - Seed crystal preparation - washing procedure

Performing secondary nucleation experiments inherently implies the use of seed crystals. This section describes how these seeds are formed and prepared for an experimental run. Special attention was paid to the washing procedure, also known as the “pretreatment step”.

Seed crystal creation

To ease handling and subject a sufficiently large crystal surface area to high fluid shear values in the experiments, seed crystals of the order of magnitude of 0.5 cm were used (see S5 - S8 for exact crystal sizes). Growing such large crystals was achieved by slow evaporation.

Relying on the solubility curves from literature^{21–24} for each chemical compound (see Figure S6), the necessary solute mass is weighed and dissolved in the corresponding solvent to achieve saturation at room temperature (25°C). The used solute compounds and solvents,

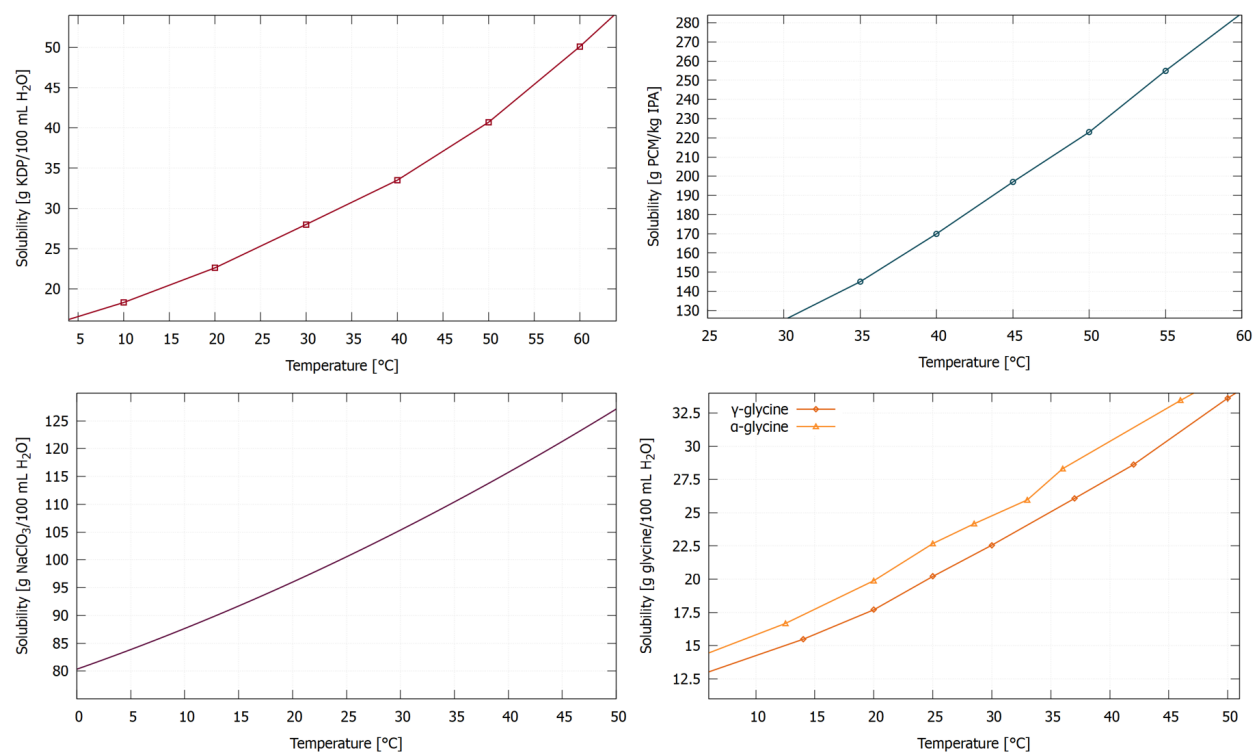


Figure S6: Solubility curves of the solute compounds used in the performed experiments (KH₂PO₄ or KDP in H₂O; PCM in IPA; NaClO₃ in H₂O; and glycine in H₂O). Values are taken from literature^{21–24} and replotted here.

KH₂PO₄ (potassium dihydrogen phosphate, Sigma Aldrich, $\geq 99.0\%$, CAS no. 7778-77-0); **PCM** (paracetamol, acetamidophenol, Acros Organics, $\geq 98\%$, CAS no. 103-90-2); **NaClO₃** (sodium chlorate, Sigma Aldrich, $\geq 98\%$, CAS no. 7775-09-9); **glycine** (Sigma Aldrich, $\geq 99\%$, CAS no. 56-40-6); **IPA** (isopropyl alcohol, 99.5%, VWR Chemicals, CAS no. 67-63-0); and **milli-Q H₂O** (18.2 M Ω ·cm⁻¹ resistivity at 25°C), were used as received.

After leaving well-stirred at 40°C for 30 min, full dissolution was achieved. The warm solution was then poured into a crystallizing dish. The large gas-liquid contact area facilitates evaporation, upping the supersaturation slowly and consistently. Only once solute crystals of the desired size are detected in the crystallizing dish, they were removed from solution using a pair of tweezers. After carefully drying them by a gentle touch from a critical task wipe (Kimtech Science), the seeds were stored in a Petri dish at ambient temperature.

The peculiar polymorphic nature of glycine²⁵ (α -glycine always forms in presence of agitation, despite γ -glycine being thermodynamically most stable), required the addition of **NaCl** (sodium chloride, Sigma Aldrich, $\geq 98\%$, CAS no. 7647-14-5). A 3:1 ratio of glycine and NaCl was selected as previous findings²⁶ suggest that these conditions are most suited for “large γ -glycine crystal formation with perfect external morphology”.

Object attachment (gluing)

Suitable seed crystals were selected based on their size and morphology (as close as possible to the size of the 3D printed object resembling an actual seed crystal). These were then glued upon the stainless steel rod/stick using a fast drying water-resistant epoxy glue (ZAP, Z-Poxy 5 minutes). Next to immobilizing the crystalline seed, also the overhead stirrers and the objects in the shape of the seed crystals were glued upon their respective stainless steel rod. An overview of all objects glued upon a stainless steel rod is provided in Figure S7.

These crystal-resembling objects and stirrers were 3D printed (FormLabs, Form 3) with Clear V4 resin (RS-F2-GPCL-04, proprietary polymethacrylate) using the technique of stereolithography. The layer thickness was set as 0.100 mm in every print. Afterwards, the print

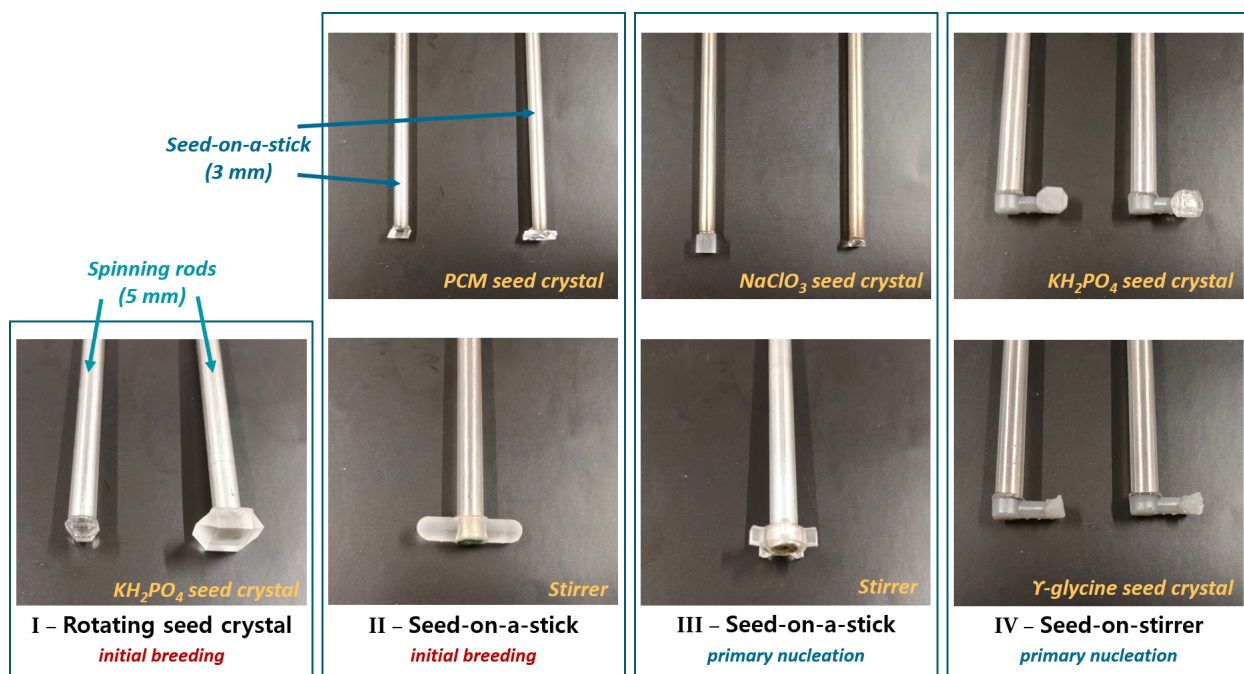


Figure S7: Overview of all objects that require washing, sorted by experiment type. In each picture with an actual crystalline seed, their 3D printed counterpart is presented as well. The initial discrepancy in size for two experimental cases (I and III) is in anticipation of the fast-growing nature of the solute compound involved (see S5 and S7).

was washed in IPA for 30 min to remove any remaining uncured resin (FormWash). The print was also cured at 60°C for 15 min (FormCure) to ensure the intended mechanical properties.

The epoxy glue, the 3D printed resin, and the stainless steel were all selected because of their non-promoting nature for crystal nucleation (no templating or enhanced heterogeneous primary nucleation effect). That in not a single experiment crystals were observed to form directly on the stirrer or seed-on-a-stick supports such a statement.

The adopted *solvent* washing procedure

To avoid initial breeding from dominating the nucleation experiments, an extensive washing procedure has been developed here. Every experimental run, all the objects relevant for the upcoming experiment (as shown in Figure S7) were routinely subjected to the following “pretreatment” steps. To ensure consistency, seed crystals already utilized in a previous experimental run were not reused: a new seed crystal was glued and washed every time.

1. The seed crystal/object attached to the rod/stick was dipped in a beaker containing pure solvent and a few times vigorously shaken up and down (crystal/object in solvent, end of the rod in researcher's hand). Close attention was paid to the crystal not touching the bottom or wall of the beaker. During this process, any crystalline debris from seed creation and storage should be dislodged and dissolved.
2. Directly after withdrawing the rod from the solvent, any solvent still adhered to the seed crystal/object is removed by a gentle touch of a critical task wipe. It was opted to not dry the seed crystal with a stream of inert gas as this might also have evaporated any solvent incorporated deeper in the seed crystal, rendering the crystal too brittle for further nucleation experiments.
3. The stainless steel rod with washed seed crystal/object is now transferred into its experimental position (slid in the corresponding slot and fixated using a screw, see Figure S2). Important to notice is that again no mechanical contact is exerted upon the seed crystal in this process.
4. The washed stainless steel rods/sticks (now immobilized upon the *motor platform unit*) were shortly after (max. 30 min waiting time) introduced into the solution. Important here is that the solution is always undersaturated (few degrees above saturation temperature). This way, the immersion of the objects (sudden puncture of the gas-liquid contact area induces undesired mixing) could not result in nucleation. Moreover, the seed crystal would also dissolve a little again, eliminating any remaining debris.
5. The solution and submerged objects were cooled down towards the desired temperature for nucleation experiments (more details, see S5 - S8). Instead of immediately starting the experiment, the solution was first kept quiescent for 15 min (regardless of the experiment type) to allow crystal growth to repair any structural defects on the crystal surface caused by the previous washing steps. As such, pristine growing crystal faces were guaranteed at the start of each experimental run.

Validation of crystalline debris removal

The work published by Steendam³ demonstrated that it is possible to visualize the crystalline fines responsible for initial breeding using scanning electron microscopy (SEM). A similar approach was adopted here to validate the developed washing procedure. The seeds were placed on electrically conductive carbon tape and coated with gold/palladium (JEOL, JFC-1300 Auto Fine Sputter Coater) before introduction into the electron microscope (JEOL, JSM-6010LV, x300 magnification). Figure S8 then shows the SEM pictures taken of both (i) an unwashed PCM seed crystal as well as (ii) a washed PCM seed crystal (last step of the washing procedure omitted because SEM does not support the analysis of wet samples).

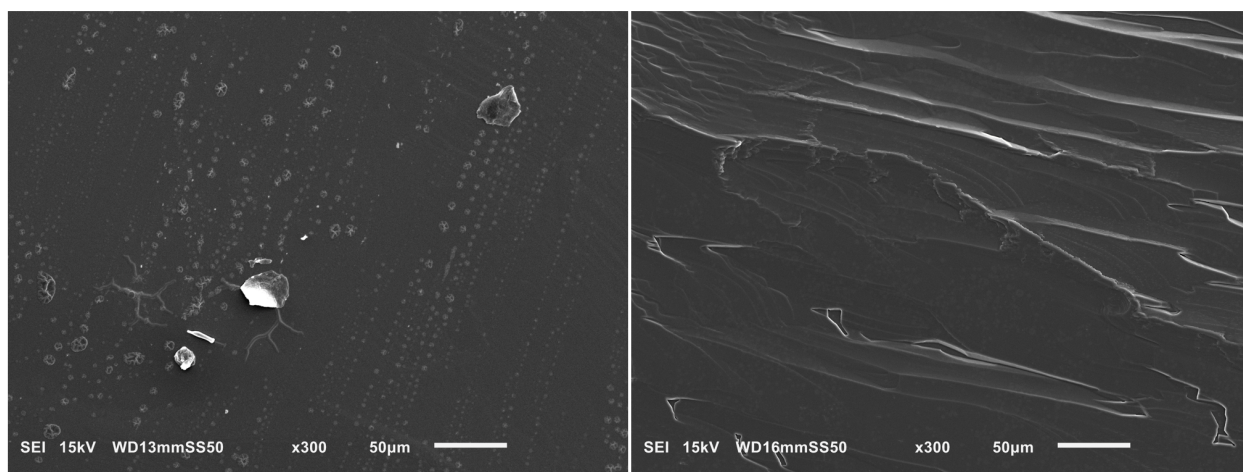


Figure S8: SEM pictures of an unwashed PCM seed crystal (**left**) and a washed one (**right**). The applied “pretreatment” is capable of removing crystalline fines causing initial breeding.

As can be seen, the surface of the unwashed crystal clearly displays debris. However, this is absent after applying the aforementioned washing procedure (minus the last step). The attentive reader can even see that the surface for the washed PCM crystals has slightly dissolved during this step, resulting in some minimal roughness of the crystal surface. This highlights the need for a healing phase in a supersaturated solution before the initializing a nucleation experiment (last step of the washing procedure above).

Validation of efficacy surface healing step

Since the washing procedure introduces some roughness on the seed crystal surface, it was decided to introduce a surface healing step before the seed crystal was subjected to high fluid shear values. Practically, this surface healing step comprises of keeping the washed seed crystal stagnant for 15 minutes in the supersaturated solution.

To ensure that the selected 15 minutes suffice to result in pristine growing crystal faces, the surface healing step was reproduced here and its effect analyzed using optical microscopy and SEM. A first clear indication that the surface healing step was long enough can be seen in Figure S9. Here, the roughness introduced from washing the KH_2PO_4 allows to identify that the surface was healed and growing at the moment rotation was commenced.

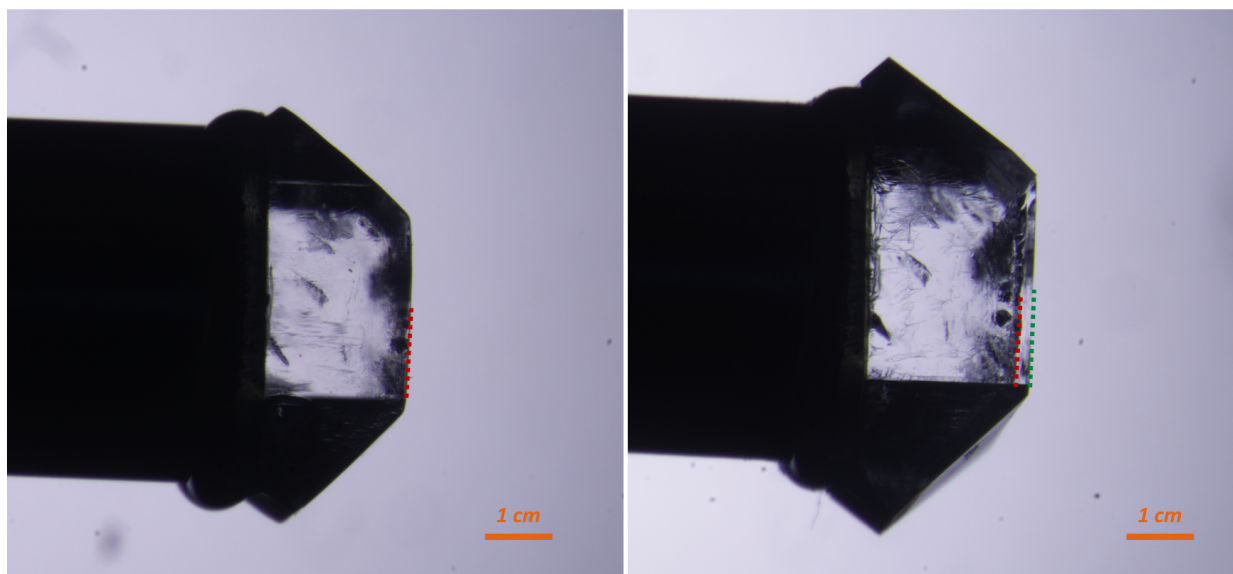


Figure S9: Optical microscopy pictures of a washed KH_2PO_4 seed crystal before (**left**) and after (**right**) the surface healing step. The small but visible extent of crystal growth indicates that a healed and growing crystal surface is present at the start of the experiment.

While the fast-growing nature of KH_2PO_4 allows to see surface healing using simple optical microscopy, SEM has to be applied for slow-growing chemical compounds such as PCM. Figure S10 displays an SEM picture of the surface of a PCM seed after a surface healing step. When comparing back to Figure S8, it is clear that the surface of the seed is again fully developed (fully flat).

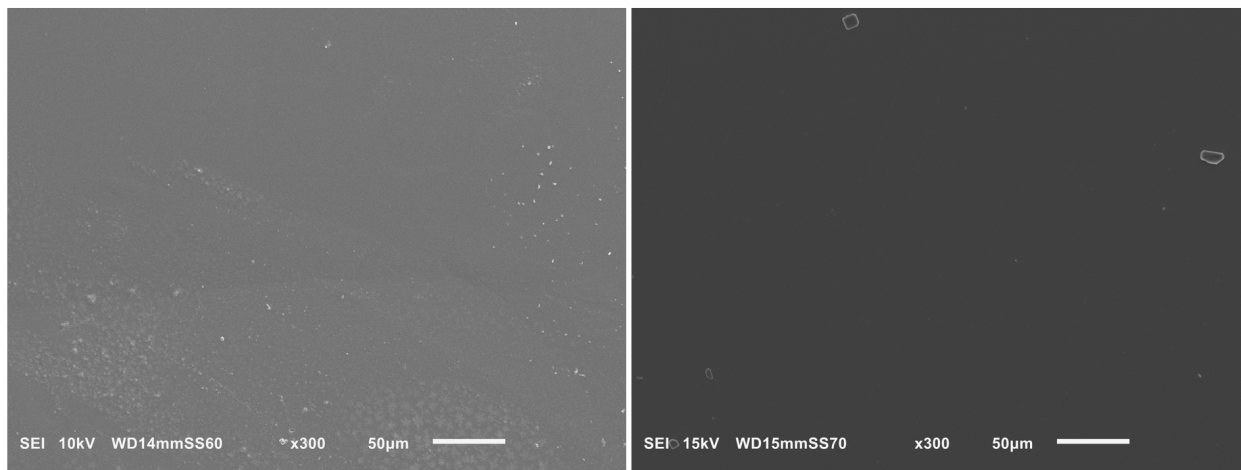


Figure S10: SEM pictures of a PCM (left) and KH_2PO_4 (right) seed crystal surface after completion of the surface healing step. In both cases, a flat crystal surface indicates a successful healing step. The visible crystalline debris results from the unavoidable removal of the seed crystal from a supersaturated solution (without applying a washing step).

Note that some pieces of crystalline debris are again visible on the crystal surface. However, these do not result from the surface healing step, but rather from the experimental procedure for SEM. Once the healed seed is removed from the supersaturated solution, attached solvent will quickly evaporate. This results in crystalline fines deposited on the flat crystal surface. A similar phenomenon took place during seed creation, requiring a washing procedure to remove these small crystalline particulates (which can cause initial breeding).

As a final validation, the seed crystal surface of a healed KH_2PO_4 seed crystal surface was also analyzed using SEM (see Figure S10). Next to the visible crystal growth, it can be seen that the surface is indeed also completely healed (fully flat).

S4 - Solution preparation and experiment initialization

Regardless of the solute and solvent used, these sections elucidate how the solution was prepared and the experimental run was initialized. The general terminology used here (indicated in *blue italics*) links to the specifics listed for each experiment type (see S5 - S8).

Solution preparation

As a first step, the borosilicate glass bottle with cap selected for solution preparation was cleaned using milli-Q water and dried with compressed air to remove any residual impurities. Next, *solute* was weighed and added to the bottle before *solvent* was poured to obtain a solution of desired *solute concentration* (and thus saturation, see Figure S6). After dissolving all solute material by keeping the solution well-stirred at a high *dissolution temperature* for 30 min (heating-stirrer plate, Teflon magnetic stir bar), the solution was filtered (Whatman Puradisc 25 Nylon filter, 0.45 μm pore size) and transferred into a second precleaned glass bottle. The filtered solution was again heated towards the *dissolution temperature* to ensure the absence of crystals. For every experimental run, a new solution was prepared.

Start-up experimental run

Before each experiment, the crystallizers were thoroughly cleaned with milli-Q water at 60°C and dried with compressed air to remove any crystalline remnants. Using the coolant water in the annular gap of the double-jacketed crystallizers, they were heated to the *preheated crystallizers temperature* to eliminate premature crystal formation on the cold wall during solution transfer. The solution was subsequently distributed among these 20 mL crystallizers using a micropipette, before lowering the *motor platform unit* with stirrer and/or seed-on-a-stick attached, and cooling the solution towards the *nucleation experiment temperature*. Upon reaching this temperature, the solution was kept quiescent for 15 min to complete seed crystal surface healing before rotation (*RPM values*) and data recording was commenced.

S5 - Characteristics of experiment I

Since the common procedures are already covered in the previous sections (see S2 - S4), this section mainly focuses on the remaining unknown specifics for experiment type I. As a quick refresher, the concept of the experiment is illustrated in Figure S11.

Experimental conditions

In correspondence with Section S4, the highlighted terms are now identified:

- *Solute*: potassium dihydrogen phosphate (KH_2PO_4)
- *Solvent*: milli-Q water (H_2O)
- *Solute concentration*: 35 g KH_2PO_4 /100 mL H_2O (saturated @ 43°C)
- *Dissolution temperature*: 50°C
- *Preheated crystallizers temperature*: 50°C
- *Nucleation experiment temperature*: 20°C
- *RPM values*: 1660 RPM (12V applied on DC motors)

A graphical representation of the adopted temperature profile is provided in Figure S12.

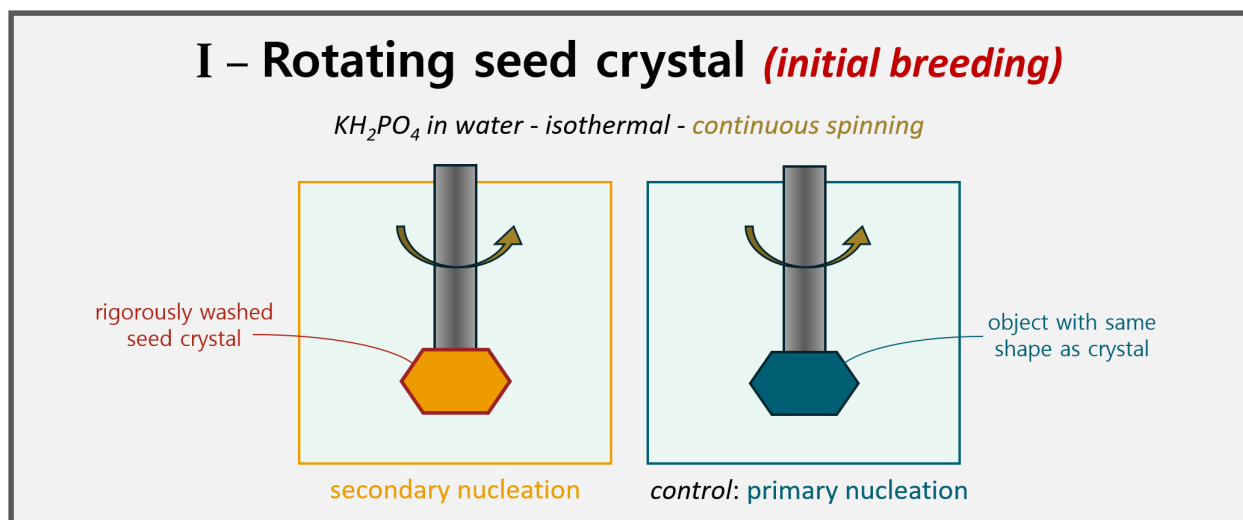


Figure S11: Schematic representation of the characteristics in experiment type I. *Detail of the overview figure from the main document.*

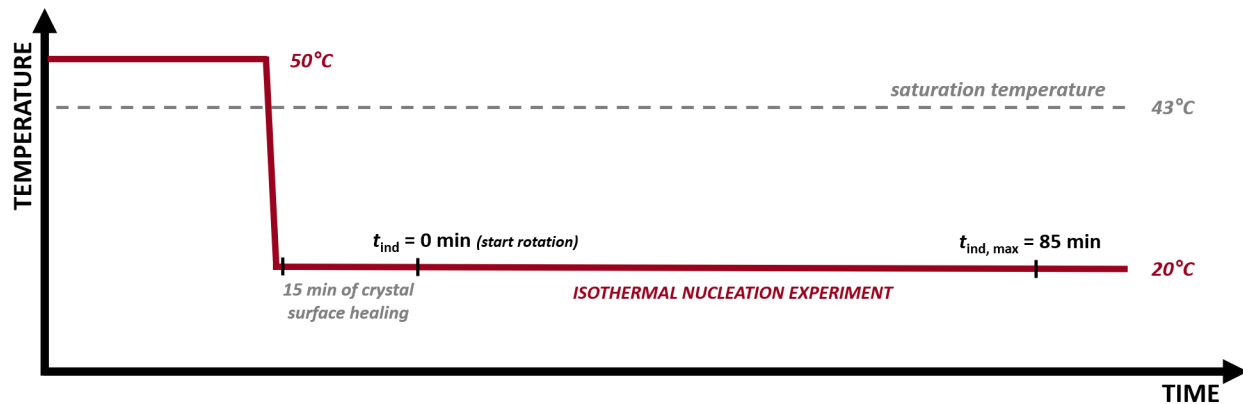


Figure S12: The temperature profile followed during runs for experiment type I. The isothermal nucleation experiments started when rotation was switched on, and ended after 85 min.

Geometrical specifications

The technical drawings in Figure S13 specify the exact dimensions of the used crystallizers and the submerged objects (experiment type I: seed crystal attached to rod). To eliminate possible bias resulting from small reactor difference in real-life, the positions of *secondary nucleation* and *primary nucleation* experiments were attributed randomly. Each run consisted of three *secondary nucleation* and two *primary nucleation* experiments (five crystallizers employed each run), to rule out outliers resulting from a single false experimental run.

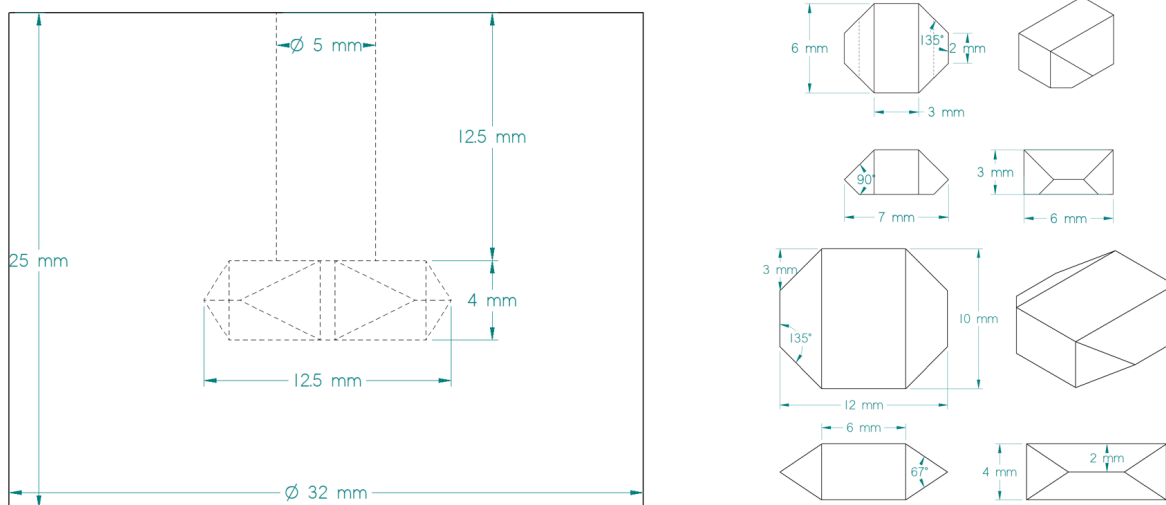


Figure S13: Technical drawings of experimental setup for experiment type I. The dimensions of the crystallizer (left), as well as the seed crystal for *secondary nucleation* experiments, and the object replacing the seed for *primary nucleation* experiments are given (right).

Anticipating fast crystal growth

The fast-growing nature of KH_2PO_4 crystals renders it challenging to accurately mimic the continuously increasing local fluid shear values exerting force on the seed crystal surface in *secondary nucleation* experiments. Therefore, the object applied in *primary nucleation* control experiments was modeled from the largest crystal size that could be achieved in *secondary nucleation* experiments: the seed size after 85 min (maximal duration). Figure S13 illustrates the exact dimensions of both the initial crystalline seed and the inert object. Due to (i) small deviations of seed crystals from the ideal dimensions as reported here and (ii) the fast-growing nature of seed crystals, *secondary nucleation* experiments are expected to show a broader confidence interval than their *primary nucleation* counterparts.

Fast crystal growth can also deplete the supersaturation essential for crystal formation during nucleation experiments. To show that this effect is negligible here, a quick back-of-the-envelope calculation was performed. Assuming a cuboid shape, the volume of the seed at start and end of an experiment can be calculated.

$$\text{start: } V = l \cdot b \cdot h = 7 \cdot 6 \cdot 3 = 126 \text{ mm}^3$$

$$\text{end: } V = l \cdot b \cdot h = 12 \cdot 10 \cdot 4 = 480 \text{ mm}^3$$

The difference between both values ($354 \text{ mm}^3 = 0.354 \text{ cm}^3$) is the volume that the seed crystal grew during the experiment. Deploying the density $\rho = 2.34 \text{ g/cm}^3$ of KH_2PO_4 , the loss of solute mass ($m = \rho \cdot V$) thus results for an absolute worst case scenario in 0.82 g, only a minor portion of the achieved supersaturation (see Figures S6 and S12). Keeping in mind that this is a large overestimation of the actual crystal size and that almost no nucleation experiments reach 85 min, it seems fair to assume that supersaturation depletion from crystal growth can be ignored.

Note on the adopted induction time approach

It is worthwhile to clarify that the usage of induction times here (Experiment I - isothermal nucleation approach) is different from the mainstream usage in crystallization literature.

In conventional literature, an induction time approach is frequently adopted to experimentally estimate the nucleation rate in a crystallizer. By repeatedly measuring how long it takes before the first crystal emerges from the clear solution, it becomes possible to determine the overall nucleation kinetics in the crystallizer at the studied conditions (supersaturation, stirring speed, etc.). Moreover, a nucleation process is inherently stochastic and it has been shown²⁷ that measured induction times follow a Poisson distribution. Building on this knowledge, the typically adopted procedure estimates the nucleation rate by fitting through the cumulative probability curve. Some research articles found in literature^{28,29} explain this conventional procedure in great detail.

In this work, the goal is not to estimate nucleation rates but to use induction times as a tool to compare the *secondary nucleation* experiments with the *primary nucleation* control experiments. Purely from its phenomenological³⁰ definition, secondary nucleation must always occur faster than primary nucleation. Furthermore, it is clearly shown in literature³¹ that secondary nucleation rates are orders of magnitude higher than primary nucleation ones. *It is thus expected that the presence of fluid shear-induced secondary nucleation in the secondary nucleation experiments would **on average** result in significantly lower induction times compared with the primary nucleation control experiments, regardless of the underlying probability distribution and possible offset times.* The presence of fluid shear-induced secondary nucleation should thus already be clear from comparing the mean induction times; an approach extensively adopted^{4,7,8,10-14,16} before in the community to indicate the existence of fluid shear-induced secondary nucleation. *Therefore, it is justified to focus on solely reporting **mean** induction times in the main document, as they already provide a sufficiently clear picture.*

S6 - Characteristics of experiment II

Since the common procedures are already covered in the previous sections (see S2 - S4), this section mainly focuses on the remaining unknown specifics for experiment type II. As a quick refresher, the concept of the experiment is illustrated in Figure S14.

Experimental conditions

In correspondence with Section S4, the highlighted terms are now identified:

- *Solute*: paracetamol (PCM)
- *Solvent*: isopropyl alcohol (IPA)
- *Solute concentration*: 18 g PCM/100 g IPA (saturated @ 42°C)
- *Dissolution temperature*: 60°C
- *Preheated crystallizers temperature*: 45°C
- *Nucleation experiment temperature*: polythermal experiments - 0.1°C/min cooling rate
- *RPM values*: 1375 RPM (10V applied on DC motors)

A graphical representation of the adopted temperature profile is provided in Figure S15.

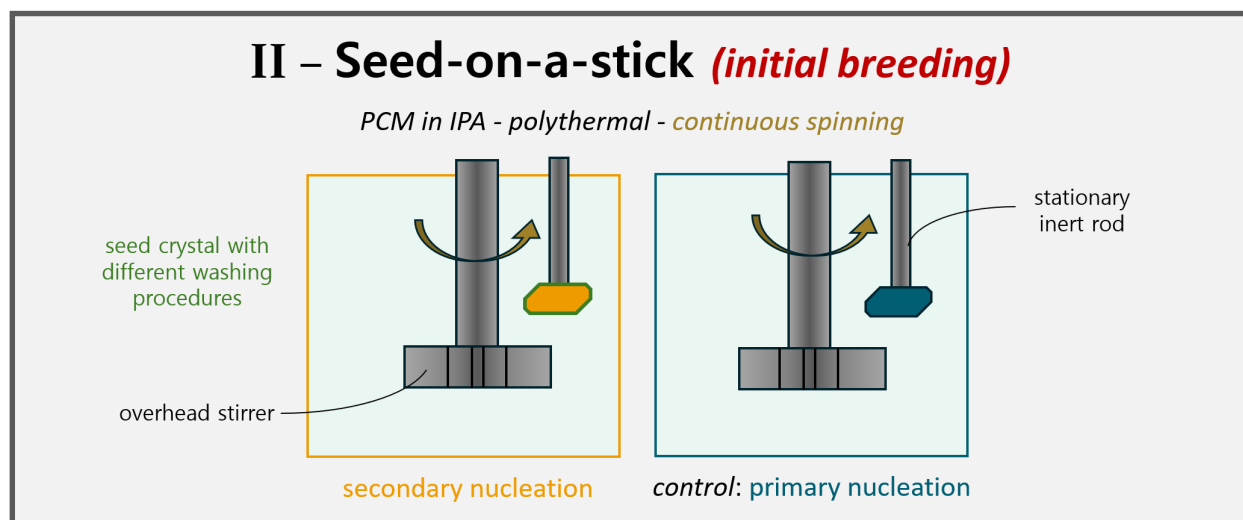


Figure S14: Schematic representation of the characteristics in experiment type II. *Detail of the overview figure from the main document.*

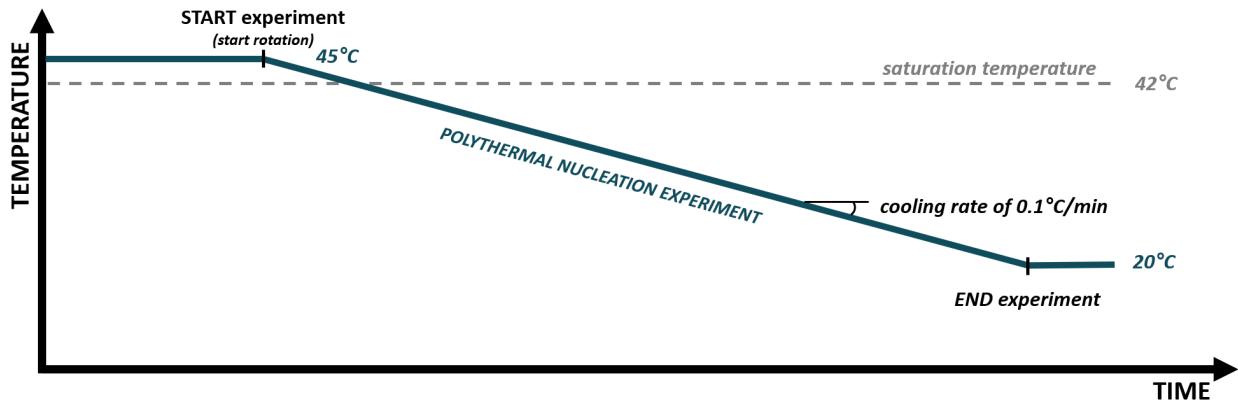


Figure S15: The temperature profile followed during runs for experiment type II. The crystal surface healing step automatically occurs once a small supersaturation is achieved. The cooling rate ($0.1^{\circ}\text{C}/\text{min}$) is slow enough that possible temperature gradients are eliminated.

Geometrical specifications

The technical drawings in Figure S16 specify the exact dimensions of the used crystallizers and the submerged objects (experiment type II: stirrer and seed-on-a-stick). To eliminate possible bias resulting from small reactor difference in real-life, the positions of *secondary nucleation* and *primary nucleation* experiments were attributed randomly. Each run consisted of a mix of *secondary nucleation* and *primary nucleation* experiments (eight crystallizers employed each run), to rule out outliers resulting from a single false experimental run.

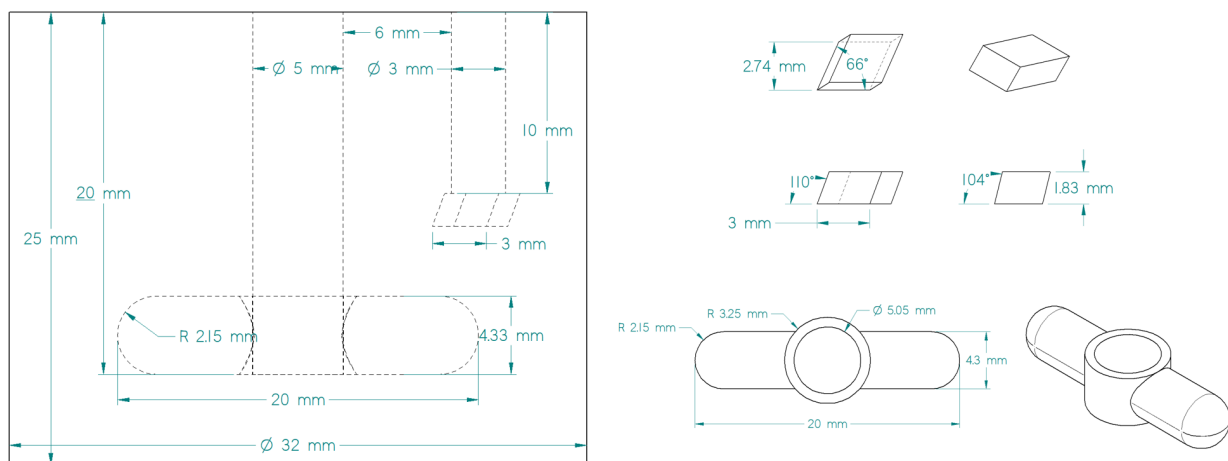


Figure S16: Technical drawings of experimental setup for experiment type II. The dimensions of the crystallizer (left), as well as the stirrer and seed crystal are given (right). The object replacing the seed in *primary nucleation* experiments has the same dimensions as the seed.

To resemble the experimental conditions from the Yousuf and Frawley paper¹⁷ as close as possible, the stirrer was modeled here to imitate a magnetic stirrer bar. However, an overhead stirrer still had to be used due to practical considerations from setup construction. Since the selected crystallizer volume here (20 mL) was also smaller compared to the one employed in their article, the location of the seed crystal was in this work nearer to the stirrer. Nevertheless, positioning it closer to the stirrer should even enhance the chances of observing fluid shear-induced secondary nucleation.

Alternative washing procedures

The use of three different seed crystal washing procedures stands central in this experiment type. While the washing procedure for the (i) *solvent washed* seed crystal is fully identical to the one listed in Section S3, the procedures of the (ii) *anti-solvent washed* and (iii) *unwashed seed* crystal differ. Where the first two steps of the procedure in the *anti-solvent washed* case are executed using an anti-solvent for paracetamol (**cyclohexane**, Sigma Aldrich, $\geq 99.0\%$, CAS no. 110-82-7), these firsts two steps are omitted for *unwashed* seed crystals.

Statistical analysis

In addition to visualizing the results (see Fig 2 in the main document), a statistical analysis of the obtained data was conducted to support our main conclusions. Since the probability distribution of data points obtained from polythermal nucleation experiments is non-Gaussian and unknown, a non-parametric test had to be adopted here. Typically in nucleation studies, a two-sample Kolmogorov-Smirnov test would be applied^{32,33} to statistically verify whether two obtained data samples come from different probability distributions or not. However, the low number of data points here ($n \leq 50$) called for the use of a modified³⁴ Kolmogorov-Smirnov test: the **two-sample Anderson-Darling test**.

For this type of statistical testing, the studied hypotheses are the following:

H_0 : The two datasets have the **same** probability distribution;

i.e. the same nucleation phenomenon is active in both datasets.

H_1 : The two datasets have a **different** probability distribution;

i.e. a different nucleation phenomenon is active in each of the two datasets.

Central in the discussion of Experiment II is whether the measured distribution from primary nucleation experiments is different from the other measured datasets. Therefore, the *primary nucleation* dataset was compared to all other datasets obtained from experiments either with *solvent washed*, *antisolvent washed*, or *unwashed* seed crystals. The resulting p values (significance level of 0.05 chosen) are 0.25, 0.01, and 0.002, respectively.

For the *antisolvent washed* and *unwashed* case, we must thus reject the null hypothesis in favor of the alternative hypothesis. It is highly likely that a different nucleation phenomenon is active (initial breeding). For the *solvent washed* case, however, there is not sufficient statistical power to reject the null hypothesis, clearly suggesting that primary nucleation is indeed the acting nucleation phenomenon in the *solvent washed* experiments, and thus hinting at a full elimination of initial breeding.

S7 - Characteristics of experiment III

Since the common procedures are already covered in the previous sections (see S2 - S4), this section mainly focuses on the remaining unknown specifics for experiment type III. As a quick refresher, the concept of the experiment is illustrated in Figure S17.

Experimental conditions

In correspondence with Section S4, the highlighted terms are now identified:

- *Solute*: sodium chlorate (NaClO_3)
- *Solvent*: milli-Q water (H_2O)
- *Solute concentration*: 100 g NaClO_3 /100 mL H_2O (saturated @25°C)
- *Dissolution temperature*: 50°C
- *Preheated crystallizers temperature*: 28°C
- *Nucleation experiment temperature*: polythermal experiments - 0.1°C/min cooling rate
- *RPM values*: 1445 RPM (10.5V applied on DC motors)

A graphical representation of the adopted temperature profile is provided in Figure S18.

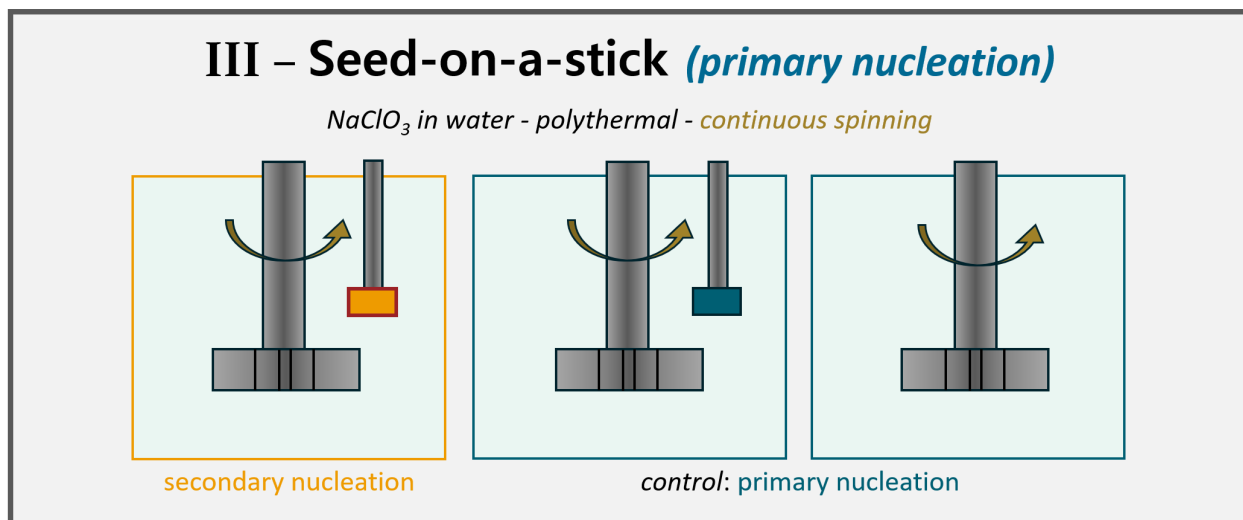


Figure S17: Schematic representation of the characteristics in experiment type III. *Detail of the overview figure from the main document.*

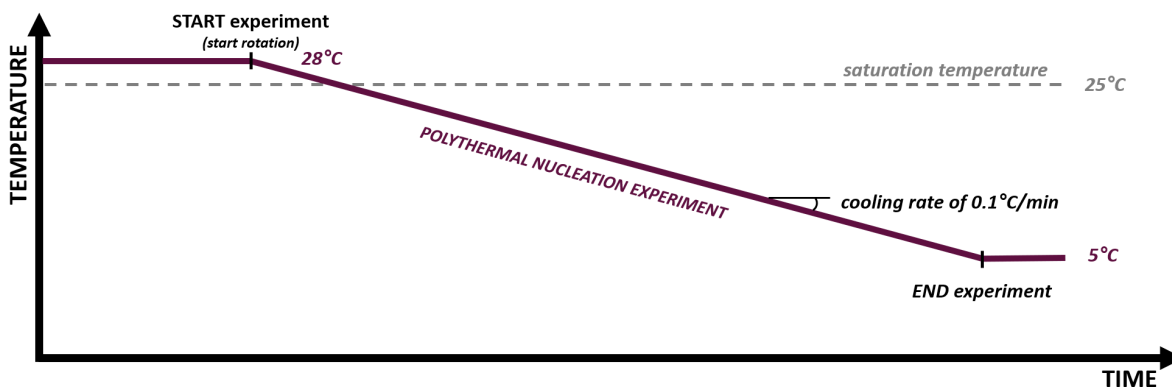


Figure S18: The temperature profile followed during runs for experiment type III. The crystal surface healing step automatically occurs once a small supersaturation is achieved (NaClO_3 is a fast grower). The cooling rate ($0.1^\circ\text{C}/\text{min}$) is slow enough that possible temperature gradients are eliminated. The experiment was stopped once a temperature of 5°C was reached.

Geometrical specifications

The technical drawings in Figure S19 specify the exact dimensions of the used crystallizers and the submerged objects (experiment type III: stirrer and seed-on-a-stick). To eliminate possible bias resulting from small reactor difference in real-life, the positions of *secondary nucleation* and *primary nucleation* experiments were attributed randomly. Each run consisted of a mix of *secondary nucleation* and *primary nucleation* experiments (eight crystallizers employed each run), to rule out outliers resulting from a single false experimental run.

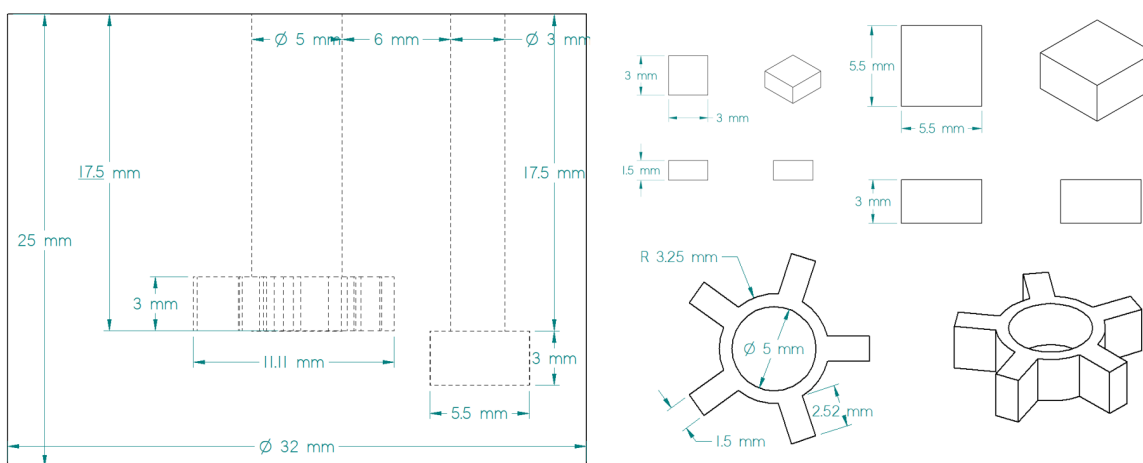


Figure S19: Technical drawings of experimental setup for experiment type II. The dimensions of the crystallizer (left), as well as the stirrer, the seed for *secondary nucleation* experiments, and the object replacing the seed for *primary nucleation* experiments are given (right).

Since there was no more need to mimic a magnetic stirrer (see Section S6), it was now opted to use a conventional Rushton turbine-like stirrer to achieve a homogeneous solution. The deployed seed crystal is located as close as possible to the stirrer to subject it to as high as possible fluid shear values. However, as can be seen in Figure S19, the optimal seed position is chosen to be slightly below the stirrer height. This is because of the fast growing nature of the NaClO_3 crystals: the seed would either grow into the stirrer or the crystallizer wall near the very end of the experiment, giving rise to unwanted attrition. The slightly lowered location of the seed crystal still allows benefiting from the enhanced fluid velocities of the lower circulation cell typically developed in a mixed vessel.

Anticipating fast crystal growth

Similarly to KH_2PO_4 , the fast-growing nature of NaClO_3 crystals poses an issue when conducting *primary nucleation* control experiments because of variable seed crystal size. Given that multiple screening tests of this experiment type were conducted, it was possible to determine the seed size at the moment that crystal formation took place in the majority of the crystallizers. These dimensions are depicted in Figure S19. Hence, the presence of a stagnant object is accurately accounted for in the primary nucleation control experiments.

Regarding possible supersaturation depletion from crystal growth, an analogous calculation as in Section S6 can be made here. Where the seed crystal volume at **start** equals 13.5 mm^3 , the volume at nucleation (**end**) equals 90.75 mm^3 . The difference between the two of $77.25 \text{ mm}^3 = 0.0773 \text{ cm}^3$ corresponds (using a density of 2.49 g/cm^3 for NaClO_3) with a solute mass loss in the solution of just 0.19 g. Referring back to Figures S6 and S18, one can see that this loss of solute mass is easily less than 10% of the present supersaturation.

Statistical analysis

In addition to visualizing the results (see Fig 3 in the main document), a statistical analysis of the obtained data was conducted to support our main conclusions. Since the probability distribution of data points obtained from polythermal nucleation experiments is non-Gaussian and unknown, a non-parametric test had to be adopted here. Typically in nucleation studies, a two-sample Kolmogorov-Smirnov test would be applied^{32,33} to statistically verify whether two obtained data samples come from different probability distributions or not. However, the low number of data points here ($n \leq 50$) called for the use of a modified³⁴ Kolmogorov-Smirnov test: the **two-sample Anderson-Darling test**.

For this type of statistical testing, the studied hypotheses are the following:

H_0 : The two datasets have the **same** probability distribution;

i.e. the same nucleation phenomenon is active in both datasets.

H_1 : The two datasets have a **different** probability distribution;

i.e. a different nucleation phenomenon is active in each of the two datasets.

Central in the discussion of Experiment III is whether the measured distribution from primary nucleation experiments (with object) is different from the other measured datasets. Therefore, the *with object* dataset was compared to all other datasets obtained from either primary nucleation experiments *without object*, or *secondary nucleation* experiments. The resulting p values (significance level of 0.05 chosen) are **0.24** and **0.08**, respectively.

In both cases, the null hypothesis cannot be rejected. Consequently, the same nucleation phenomenon must be active in all three experimental datasets (i.e. primary nucleation). The observed lower p value should be attributed to noise introduced by experimental errors (cooling profile was stopped at 5°C for practical reasons, distorting the sample distribution).

Optical activity of NaClO₃

To determine the chirality of formed NaClO₃ crystals (levorotatory *l* or dextrorotatory *d*), an optical microscope (SMZ25, Nikon) was equipped with two linear polarization filters (LPVISE200-A, Thorlabs). Before transmission through the crystals, the light was polarized using the first filter (i.e. the polarizer). After passing through the crystalline sample, the light was again polarized using the second filter (i.e. the analyzer) before it reached the camera of the microscope (DS-Fi3, Nikon). By rotating the analyzer relative to the polarizer, the different enantiomers of NaClO₃ turned either dark or bright. The relative rotation of the polarizers was kept the same for all analyzed crystals. A typical example on how the handedness of formed NaClO₃ crystals was detected, is shown in Figure S20.

The chirality of NaClO₃ crystals is often used in nucleation experiments to determine whether primary or secondary nucleation is dominant. When primary nucleation is dominant, a racemic mixture of *l*-NaClO₃ and *d*-NaClO₃ is formed. When secondary nucleation dominates, it is expected that the formed crystals exhibit the same handedness as the seed crystal. This concept is visually depicted in Figure S21.

Pivotal in this reasoning is that secondary nucleation, as per usual, is dominated by attrition. In the experiments conducted in this work, however, attrition was avoided in favor of fluid shear-induced secondary nucleation. Because the latter assumes that secondary

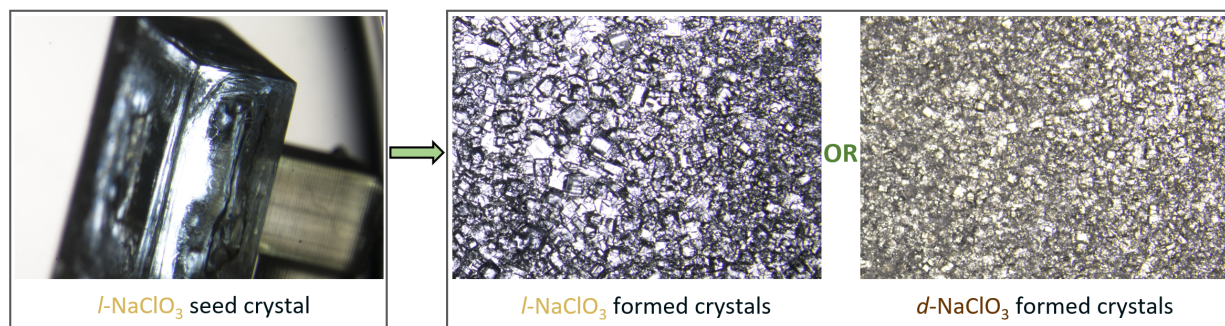


Figure S20: Visualization on how the chirality of the formed NaClO₃ crystals was determined using polarization microscopy. The detected color (bright or dark) reveals the chirality of both the seed crystal and the formed crystals. The crystals formed in a single crystallizer always displayed the same color (pictures on the right come from different experiments).

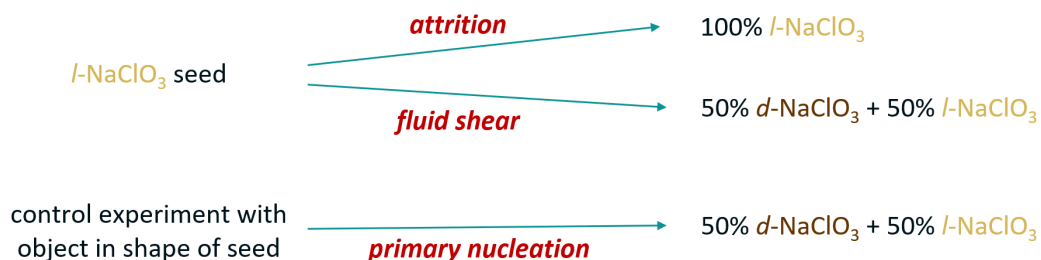


Figure S21: While attrition-dominated secondary nucleation experiments result in the formation of secondary crystals with the same chirality as the seed, fluid shear-induced secondary nucleation results in a racemic mixture of *l*-NaClO₃ and *d*-NaClO₃.

crystals originate from *aggregates* that are present in the crystal-solution boundary layer, it is expected that a racemic mixture of *l*-NaClO₃ and *d*-NaClO₃ is formed. Since there is no contact between the *aggregates* and the seed crystal surface, there is no reason why the formed crystals should have a handedness related to the used seed crystal.

When looking at the obtained results (see Fig S22), the results for primary nucleation experiments are as expected (trending towards racemic mixture of *l*-NaClO₃ and *d*-NaClO₃, limited data numbers skew the balance). For secondary nucleation experiments, *the main observation is that a substantial number of experiments formed crystals with a different chirality than the seed crystal. This observation does not support the existence of fluid shear-induced secondary nucleation (i.e. primary nucleation takes place instead), but neither does it serve as proof against it.*

Primary nucleation experiments		Secondary nucleation experiments			<div style="border: 1px solid black; padding: 5px; font-size: small;"> <i>only crystals of one chirality detected in each crystallizer → attrition takes over after formation of first crystal</i> </div>
Chirality of seed crystal	Number of events	Chirality of seed crystal	Chirality of formed crystals	Number of events	
<i>l</i>	22	<i>l</i>	<i>l</i>	7	} 12 secondary crystals with SAME chirality as seed
<i>d</i>	13	<i>d</i>	<i>d</i>	5	
approaching 50/50 <i>d</i> -NaClO ₃ / <i>l</i> -NaClO ₃		<i>l</i>	<i>d</i>	2	} 6 secondary crystals with DIFFERENT chirality than seed
		<i>d</i>	<i>l</i>	4	

Figure S22: Overview of the obtained chirality of formed crystals. The main observation is the formation of secondary crystals with a different chirality than the used seed crystal.

S8 - Characteristics of experiment IV

Since the common procedures are already covered in the previous sections (see S2 - S4), this section mainly focuses on the remaining unknown specifics for experiment type IV. As a quick refresher, the concept of the experiment is illustrated in Figure S23.

Experimental conditions

In correspondence with Section S4, the highlighted terms are now identified:

- *Solute*: glycine or potassium dihydrogen phosphate (KH_2PO_4)
- *Solvent*: milli-Q water (H_2O)
- *Solute concentration*: 25-27 g glycine/100 mL H_2O or 33-35 g KH_2PO_4 /100 mL H_2O
- *Dissolution temperature*: 50°C
- *Preheated crystallizers temperature*: 50°C (always above saturation temperature)
- *Nucleation experiment temperature*: 18.5°C or 20°C
- *RPM values*: custom spinning profile

A graphical representation of the adopted temperature profile is provided in Figure S24.

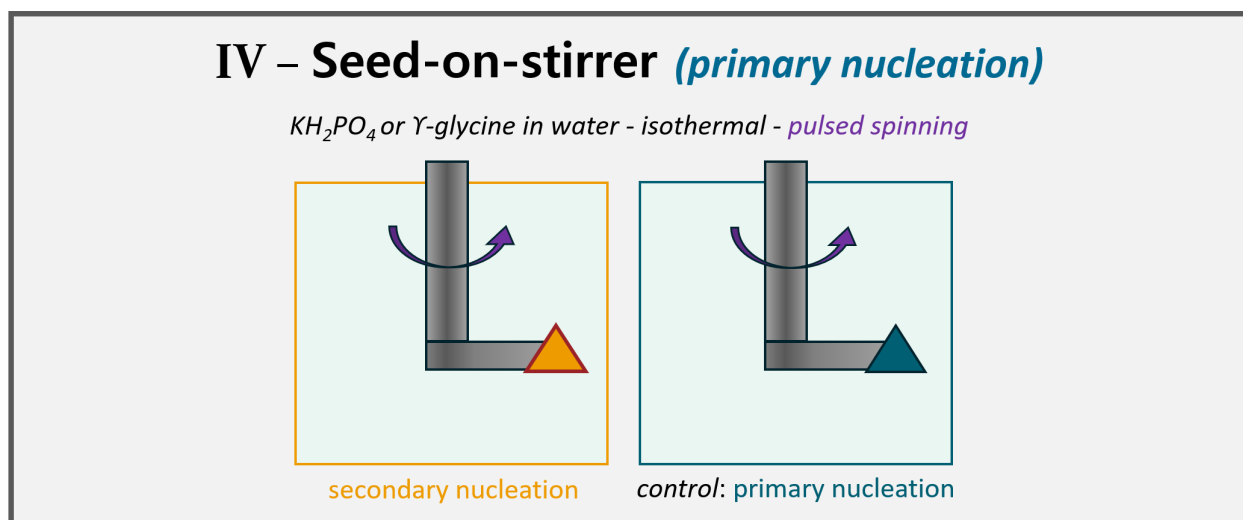


Figure S23: Schematic representation of the characteristics in experiment type IV. *Detail of the overview figure from the main document.*

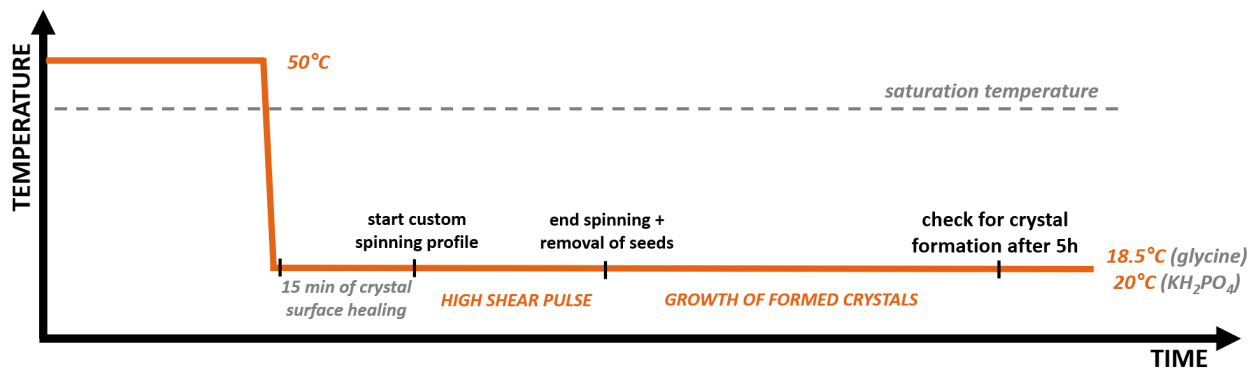


Figure S24: The temperature profile followed during runs for experiment type IV. After applying the high shear pulse step, the solution was kept quiescent for 5 h to let potentially nucleated crystals grow to a detectable size. Whether or not crystals were formed in any of the five crystallizers of one experimental run was analyzed by visual inspection (naked eye).

Geometrical specifications

The technical drawings in Figure S25 specify the exact dimensions of the used crystallizers and the submerged objects (experiment type IV: seed crystal attached to rod). To eliminate possible bias resulting from small reactor difference in real-life, the positions of *secondary nucleation* and *primary nucleation* experiments were attributed randomly. Each run consisted of a mix of five *secondary nucleation* and five *primary nucleation* experiments (ten crystallizers used each run), allowing to isolate issues caused by a single experimental run.

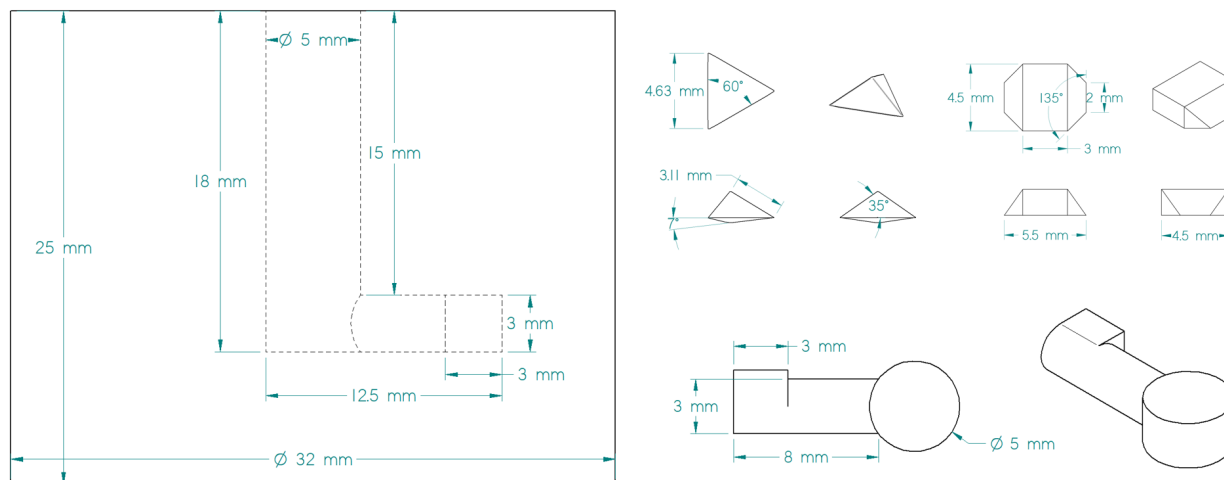


Figure S25: Technical drawings of experimental setup for experiment type IV. The dimensions of the crystallizer (left), as well as the stirrer and seeds are given (right). The object replacing the seed in *primary nucleation* experiments has the same dimensions as the seed.

Custom spinning profile

To generate the needed high fluid shear values, the spinning profile as portrayed in Figure S26 was adopted here. The most prominent characteristic is the repeated occurrence of high shear pulses to up the chances of fluid shear-induced secondary nucleation to occur, while also having a delay in between for possible regeneration of the *crystal-solution boundary layer*. Power and duration of these pulses (max RPM values) were selected as high as possible while still avoiding excessive deformation of the air-solution surface layer in the crystallizer. The duration of the full pattern (2 min) was kept short too avoid attrition of crystals formed during the first pulses of the pattern.

Another characteristic of the applied profile is the slow spinning action of the seed crystals during the surface healing step. This step does not have as purpose to ensure the absence of initial breeding (see S3; quiescent healing was proven to be already sufficient), but rather to scrutinize yet another possible hypothesis from literature. The work from Tai and Chang¹⁶ claims that a high interfacial concentration is needed for *aggregate* regeneration and thus fluid-shear secondary nucleation to occur. By spinning the seed crystal glued on the stirrer, this interfacial concentration is elevated right before the high shear pulses.

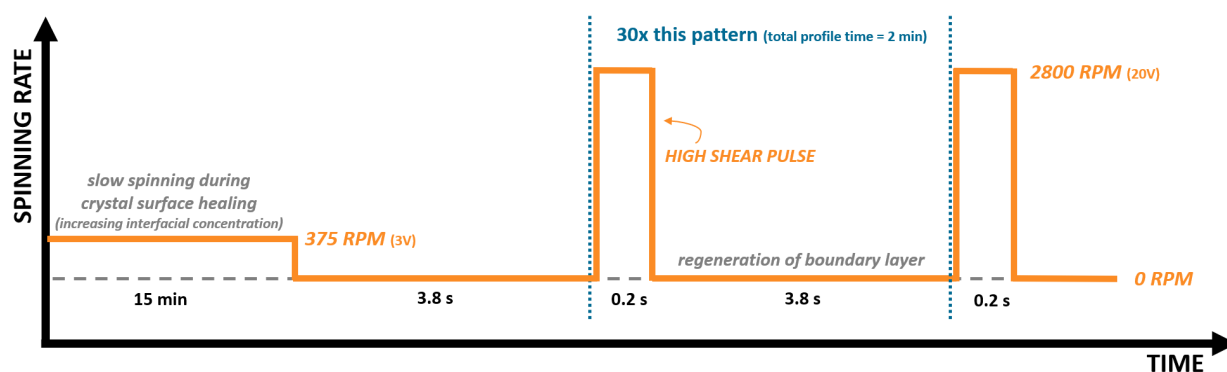


Figure S26: The spinning profile applied as high shear pulse step during runs for experiment type IV. By slowly spinning the seed crystal during the surface healing step, a higher interfacial concentration is established. After the high shear pulse, a time interval is reserved for the possible regeneration of *aggregates* in the crystal-solution boundary layer.

Polymorphic behavior of glycine

To validate whether the used seed crystals were of the intended γ -glycine form, Raman spectra of the deployed seeds were acquired using a confocal Raman microscope (MonoVista CRS+, S&I Instruments). The 532 nm green excitation laser source (Cobolt Samba) was focused using a LWD 50 \times 0.8 NA objective lens (MXPLFLN50X, Olympus). The backward Raman scattering signal (collected via the same objective lens) passed through a 100 μm confocal pinhole before being heading towards a monochromator (Princeton Instruments) equipped with a 400 grooves/nm grating. The resulting signal was recorded with a charge-coupled camera device (Newton 920, Andor).

Furthermore, the use of γ -glycine as seed crystal allows exploiting the polymorphic nature of glycine (see S3). Crystals formed during the nucleation experiments were also analyzed and found all to be α -glycine. The reference spectra of both polymorphs is given in Figure S27. This formation of only α -glycine (even when seeded with γ -glycine) was to be expected since mixing was present in the system²⁵ and is thus no example of cross-nucleation. Alternatively, the observed formation of α -glycine also does not prove that primary nucleation was present in the conducted secondary nucleation experiments. Secondary nucleation from fluid shear assumes no contact between *aggregates* in the boundary layer and the seed crystal surface.

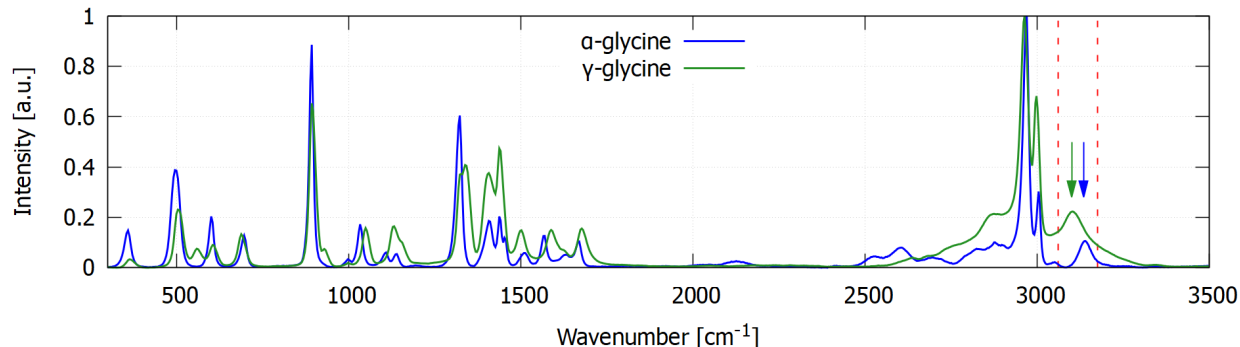


Figure S27: Reference Raman spectra of the relevant polymorphs of glycine in this study. Though the seed crystals were γ -glycine, all crystals formed in the experiments were α -glycine. However, this should not be considered as an instance of cross-nucleation as the (substantial) mixing present in this work hinders the formation of γ -glycine.

References

- (1) Lal, D.; Mason, R.; Strickland-Constable, R. Collision breeding of crystal nuclei. *Journal of Crystal Growth* **1969**, *5*, 1–8.
- (2) Tait, S.; White, E. T.; Litster, J. D. A Study on Nucleation for Protein Crystallization in Mixed Vessels. *Crystal Growth & Design* **2009**, *9*, 2198–2206.
- (3) Steendam, R. R.; Frawley, P. J. Secondary nucleation of sodium chlorate: the role of initial breeding. *Crystal Growth & Design* **2019**, *19*, 3453–3460.
- (4) Powers, H. E. C. Growth of sucrose crystals. *Nature* **1956**, *178*, 139–140.
- (5) Denk, E. G.; Botsaris, G. D. Fundamental studies in secondary nucleation from solution. *Journal of Crystal Growth* **1972**, *13-14*, 493–499.
- (6) Clontz, N. A.; Johnson, R. T.; McCabe, W. L.; Rousseau, R. W. Growth of magnesium sulfate heptahydrate crystals from solution. *Industrial & Engineering Chemistry Fundamentals* **1972**, *11*, 368–373.
- (7) Sung, C. Y.; Estrin, J.; Youngquist, G. R. Secondary nucleation of magnesium sulfate by fluid shear. *AIChE Journal* **1973**, *19*, 957–962.
- (8) Estrin, J.; Wang, M. L.; Youngquist, G. R. Secondary nucleation due to fluid forces upon a polycrystalline mass of ice. *AIChE Journal* **1975**, *21*, 392–395.
- (9) Jagannathan, R.; Sung, C.; Youngquist, G.; Estrin, J. Fluid shear secondary nucleation of magnesium sulfate and potassium aluminum sulfate. *AIChE Symposium Series* **1980**, *76*, 90–97.
- (10) Wang, M.; Yang, H. Secondary nucleation of ϵ -caprolactam in toluene solution by fluid shear forces. *Chemical Engineering Communications* **1981**, *12*, 241–251.

- (11) Wang, M.; Huang, H.; Estrin, J. Secondary nucleation of citric acid due to fluid forces in a Couette flow crystallizer. *AIChE Journal* **1981**, *27*, 312–315.
- (12) Youngquist, G. *Crystallization and Precipitation*; Elsevier, 1987; pp 45–51.
- (13) Wang, J.; Estrin, J. Secondary nucleation of sucrose by fluid shear in aqueous solutions. *Chemical Engineering Communications* **1996**, *152-153*, 275–286.
- (14) Qian, R.-Y.; Botsaris, G. D. Nuclei breeding from a chiral crystal seed of NaClO₃. *Chemical Engineering Science* **1998**, *53*, 1745–1756.
- (15) Buhse, T.; Durand, D.; Kondepudi, D.; Laudadio, J.; Spilker, S. Chiral symmetry breaking in crystallization: the role of convection. *Physical Review Letters* **2000**, *84*, 4405–4408.
- (16) Tai, C. Y.; Tai, C.-D.; Chang, M.-H. Effect of interfacial supersaturation on secondary nucleation. *Journal of the Taiwan Institute of Chemical Engineers* **2009**, *40*, 439–442.
- (17) Yousuf, M.; Frawley, P. J. Experimental evaluation of fluid shear stress impact on secondary nucleation in a solution crystallization of paracetamol. *Crystal Growth & Design* **2018**, *18*, 6843–6852.
- (18) Cashmore, A.; Georgoulas, K.; Boyle, C.; Lee, M.; Haw, M. D.; Sefcik, J. Secondary nucleation of α -glycine induced by fluid shear investigated using a Couette flow cell. *Crystal Growth & Design* **2024**, *24*, 4975–4984.
- (19) Qian, R.-Y.; Botsaris, G. D. A new mechanism for nuclei formation in suspension crystallizers: the role of interparticle forces. *Chemical Engineering Science* **1997**, *52*, 3429–3440.
- (20) Tai, C. Y.; Wu, J.-F.; Rousseau, R. W. Interfacial supersaturation, secondary nucleation, and crystal growth. *Journal of Crystal Growth* **1992**, *116*, 294–306.

- (21) Zhang, Y.; Dai, Y.; Tie, G.; Hu, H. Effects of temperature on the removal efficiency of KDP crystal during the process of magnetorheological water-dissolution polishing. *Applied Optics* **2016**, *55*, 8308.
- (22) Granberg, R. A.; Rasmuson, Å. C. Solubility of Paracetamol in Pure Solvents. *Journal of Chemical & Engineering Data* **1999**, *44*, 1391–1395.
- (23) Mayer, C.; Lacmann, R. Secondary nucleation of sodium chlorate studied with the aid of asymmetric crystallization. *Chemical Engineering & Technology* **1997**, *20*, 633–640.
- (24) Yang, X.; Wang, X.; Ching, C. B. Solubility of Form α and Form γ of Glycine in Aqueous Solutions. *Journal of Chemical & Engineering Data* **2008**, *53*, 1133–1137.
- (25) Vesga, M. J.; McKechnie, D.; Mulheran, P. A.; Johnston, K.; Sefcik, J. Conundrum of γ glycine nucleation revisited: to stir or not to stir? *CrystEngComm* **2019**, *21*, 2234–2243.
- (26) Ashok Kumar, R.; Ezhil Vizhi, R.; Vijayan, N.; Rajan Babu, D. Structural, dielectric and piezoelectric properties of nonlinear optical γ -glycine single crystals. *Physica B: Condensed Matter* **2011**, *406*, 2594–2600.
- (27) Jiang, S.; ter Horst, J. H. Crystal Nucleation Rates from Probability Distributions of Induction Times. *Crystal Growth & Design* **2011**, *11*, 256–261.
- (28) Kulkarni, S. A.; Kadam, S. S.; Meekes, H.; Stankiewicz, A. I.; ter Horst, J. H. Crystal Nucleation Kinetics from Induction Times and Metastable Zone Widths. *Crystal Growth & Design* **2013**, *13*, 2435–2440.
- (29) Briuglia, M. L.; Sefcik, J.; ter Horst, J. H. Measuring Secondary Nucleation through Single Crystal Seeding. *Crystal Growth & Design* **2019**, *19*, 421–429.

- (30) Threlfall, T. L.; Coles, S. J. A perspective on the growth-only zone, the secondary nucleation threshold and crystal size distribution in solution crystallisation. *CrystEngComm* **2016**, *18*, 369–378.
- (31) Cashmore, A.; Miller, R.; Jolliffe, H.; Brown, C. J.; Lee, M.; Haw, M. D.; Sefcik, J. Rapid Assessment of Crystal Nucleation and Growth Kinetics: Comparison of Seeded and Unseeded Experiments. *Crystal Growth & Design* **2023**, *23*, 4779–4790.
- (32) Devos, C.; Van Gerven, T.; Kuhn, S. Nucleation kinetics for primary, secondary and ultrasound-induced paracetamol crystallization. *CrystEngComm* **2021**, *23*, 5164–5175.
- (33) Little, L. J.; Sear, R. P.; Keddie, J. L. Does the γ Polymorph of Glycine Nucleate Faster? A Quantitative Study of Nucleation from Aqueous Solution. *Crystal Growth & Design* **2015**, *15*, 5345–5354.
- (34) Scholz, F. W.; Stephens, M. A. K-Sample Anderson-Darling Tests. *Journal of the American Statistical Association* **1987**, *82*, 918.